arXiv:astro-ph/0501405v1 19 Jan 2005

s Process in low-mass Asymptotic Giant Branch Stars

Oscar Straniero [a,b] Roberto Gallino [c,d] Sergio Cristallo [a,b]

[a] *INAF-Osservatorio Astronomico di Collurania and Universita' di Teramo, via M. Maggini, 64100 Teramo, Italy*

[b] *INFN-Sezione di Napoli, Complesso Universitario di Monte Sant'Angelo, Via Cintia, 80126 Napoli, Italy*

[c] *Dipartimento di Fisica Generale, Universita' di Torino, INFN-Sezione di Torino, via P. Giuria 1, 10125 Torino, Italy*

[d] *Centre for Stellar and Planetary Astrophysics, School of Mathematical Sciences, Monash University, 3800 Victoria, Australia*

Abstract

The main component of the s process is produced by low mass stars ($1.5 \leq M/M_{\odot} \leq 3$), when they climb for the second time the red giant branch and experience a series of He shell flashes called thermal pulses. During the relatively long period (10^5 yr) that elapses between two subsequent thermal pulses, a slow neutron flux is provided by the ^{13}C(α,n)^{16}O reaction taking place within a thin ^{13}C pocket located in the He-rich and C-rich mantel of these stars. A second, marginal, neutron burst occurs during the thermal pulse and it is powered by the ^{22}Ne(α,n)^{25}Mg reaction. We review the present status of the nucleosynthesis models of low mass AGB stars. The advance in the knowledge of the complex coupling between convective mixing and nuclear process, which allows the surface enrichment of C and s-process elements, is presented, together with the hypotheses concerning the physical mechanism driving the formation of the ^{13}C pocket. In order to illustrate the capabilities and the limits of the theory, an updated computation of a 2 $M_{\odot}$ stellar structure with solar chemical composition is reported. This model has been obtained by including a full nuclear network (from H up to Bi, at the termination point of the s-process path) into the stellar evolution code. The predicted modification of the surface composition occurring during the AGB evolution is shown. The new challenge of AGB modeling, namely the study of C-rich and s-rich very metal-poor stars, is discussed.

Key words: nucleosynthesis; s process; AGB stars

1 Introduction

It was in 1868 when the Jesuit astronomer Father Angelo Secchi first recognized in the peculiar spectrum of some red giants the signature of carbon enhancement [111]. This new class includes stars belonging to the Disk of the Milky Way, called by Secchi "red carbon stars" and nowaday named C(N-Type) stars, that are evolved low mass red giants with photospheric C/O $>$ 1. In the Hertzsprung-Russell diagram, they are located near the tip of the asymptotic giant branch (AGB) and represent the end point of the evolutionary sequence of a star that starts the AGB as an M giant (typically C/O $\approx$ 0.5) and progressively modifies its surface composition, passing through the MS, S and C(N) stages. The internal structure of these giant stars is made of three regions: a compact C-O core, a thin He-rich and C-rich mantel (He intershell) and an expanded H-rich envelope. As usual for red giant stars, the envelope is largely unstable against convection. Carbon is synthesized by the 3α reactions that burn at the base of an He-rich layer surrounding the core. The first question for the theoreticians was the search for a process capable to move the C from the deep interior of the star to the surface ([68], [87], [113]). Modern studies have clarified that the dredge up of C is due to the combination of two distinct convective episodes. The first is responsible for an efficient mixing of the whole He-rich layer and the second partially overlaps the zone previously mixed by the first convective episode and extends to the stellar surface. As a consequence of these two convective episodes, other products of the nucleosynthesis occurring within the He-rich mantel, besides ^{12}C, should appear at the surface. As a matter of fact, MS, S, C(N) and post-AGB stars are enriched in s-process elements, like Sr, Y, Zr, and Ba, La, Ce, Nd corresponding to the light and heavy s-abundance peaks, as early encoded by [16]. Detection of unstable ^{99}Tc, whose half life is "only" 2.1×10^5 yr, demonstrates that this enhancement cannot be due to an anomalous pollution of the pristine material from which these stars were born, but that the s process must be at work in their interiors [89]. In addition, it was realized that only relatively faint AGB stars become C-rich and that the brightest AGBs are N-rich [129]. This evidence supports the hypothesis that C(N)-stars have low mass progenitors. In massive AGBs, indeed, the CN-cycle taking place at the base of the external convective layer converts most of the C dredged up into N.

Recent studies have demonstrated that the AGB stars with $M < 3\ M_\odot$ are the major contributors to the galactic production of the isotopes belonging to the main component of the s process, involving isotopes with atomic mass beyond $A \sim 80$ (see for a review [128]). Clayton [31] first pointed out that a multiple neutron exposure, rather than a single exposure, is needed to reproduce the main component and [121] suggested that this condition could occur in the He-rich layer of an AGB star. A few years before, indeed, [110] discov-

ered that during the late AGB the He burning shell is recurrently switched on and off. At each He reignition, a thermonuclear runaway (thermal pulse) occurs and the rapid release of nuclear energy induces the formation of an extended convective region, where the products of the nucleosynthesis are fully mixed. Following the original idea of [121], the partial overlap of the convective regions recurrently generated by the thermal pulses ensures the required multiple neutron exposure (see Figure 1).

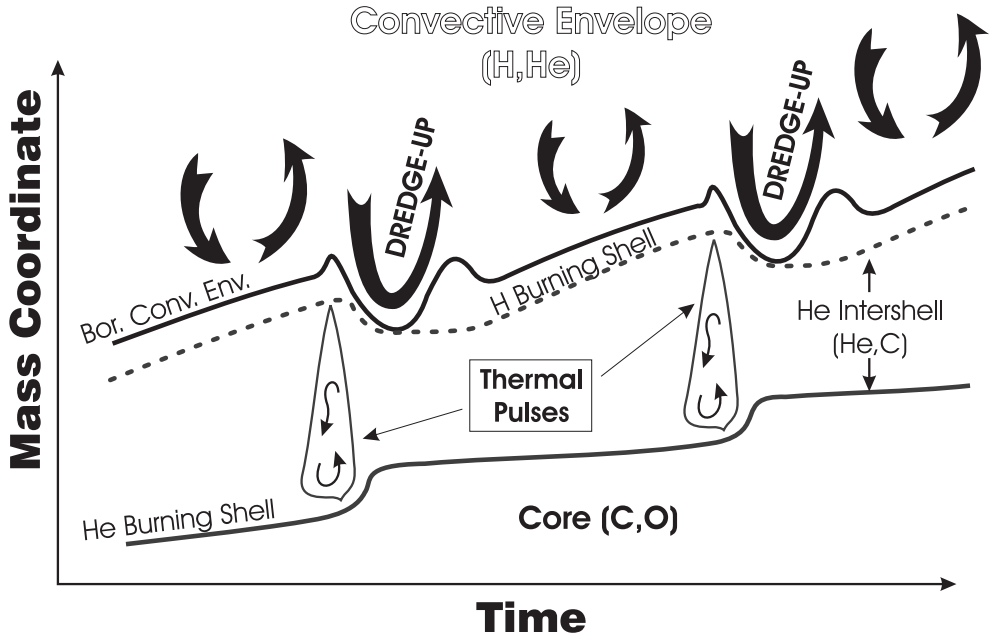

Fig. 1. This sketch illustrates the evolution of the positions of the inner border of the convective envelope, the H-burning shell and the He-burning shell, during the thermally pulsing AGB phase. The convective regions generated by two subsequent thermal pulses are also shown. Note that the temporal developments of thermal pulses and of following TDU episodes are off scale with respect to the interpulse period (see Figure 3 and 8).

Two promising neutron sources for the build up of the heavy s-process isotopes were early recognized ([21], [22]): the ^{22}Ne(α,n)^{25}Mg and the ^{13}C(α,n)^{16}O reactions. On the basis of detailed AGB stellar models, it has been understood that the major source of neutrons in low mass AGB stars is provided by the ^{13}C(α,n)^{16}O reaction. The s-process nucleosynthesis mostly occurs during the relatively long interpulse period (namely the time elapsed between two subsequent thermal pulses), in a thin radiative layer at the top of the He intershell ($\sim 10^{-3}\ M_{\odot}$), when the temperature ranges between 80 and 100 $\times\ 10^6$ K [116]. A second neutron burst giving rise to a small neutron exposure [1], but with a high peak neutron density, is released by the marginal activation of the ^{22}Ne

[1] We define the neutron exposure $\tau = \int n_n v_{th} dt$ as the time integrated neutron flux, where n_n is the neutron density and v_{th} the thermal velocity.

neutron source in the convective thermal pulse, modifying the final s-process composition at branchings along the s path depending on the neutron density or on temperature.

In this paper we discuss the present status of the extant studies of nucleosynthesis and evolution in low mass AGB stars. The AGB evolution is reviewed in sections 2 and 3. In section 4 the general problem of the third dredge up efficiency in low mass AGBs of different mass and metallicity is discussed. An attempt to properly evaluate the mass loss rate, a quantity that significantly affects the AGB evolution and nucleosynthesis, is presented in section 5. In section 6 the problem of the source of neutrons is afforded in some detail, with particular emphasis to the physical process driving the formation of a ^{13}C pocket in the He-rich and ^{12}C-rich intershell. An AGB stellar model of initial mass $M = 2\ M_{\odot}$ and solar metallicity, computed by coupling a stellar evolution code with a full nuclear network (from H to Bi), is described in section 9. Finally, among the many aspects related to the s-process nucleosynthesis occurring in AGB stars, we focus, in section 10, on one of the presently most debated problems in the field, i.e. the expected s-process nucleosynthesis for the most metal-poor stars in the Milky Way.

2 Approaching the Thermally Pulsing AGB

In stars less massive than $\sim 10\ M_{\odot}$, central He burning leaves a compact C-O core. After He exhaustion, the central density rapidly increases (above 10^5 and up to 10^8 g/cm^{-3}), electrons become highly degenerate and a huge energy loss by plasma neutrinos takes place. The neutrino energy depletion is only partially supplied by the release of gravitational energy from the core contraction, and the thermal content of the core is used to balance the deficit. The resulting cooling starts from the center, where the density is higher, and the maximum temperature moves progressively outward. It exists a maximum mass, called M_{up}, for which the whole core cools down, a fact that prevents carbon ignition. The precise value of M_{up} depends on the chemical composition: it is $\sim$7 $M_{\odot}$ for population I stars (of nearly solar composition) and for very metal-poor stars (population III), while it is smaller ($\sim$6 $M_{\odot}$) for population II (halo) stars. Stars with mass slightly larger than $M_{\rm up}$ suffer a violent carbon ignition in degenerate condition ([40], [103]). Stars with smaller mass enter the thermally pulsing AGB phase (see [38] for an updated presentation of the pre-AGB evolution).

The evolutionary track in the HR diagram calculated for a 2 $M_{\odot}$ star of solar metallicity is reported in Figure 2. The computation has been started from a homogeneous structure with a mass fraction of helium $Y = 0.275$ and a metal-

licity $Z = 0.015$ [2]. The mass fractions of all the elements beyond hydrogen and helium relative to Z have been derived from [4], except for C and N [3] and O, Ne and Ar [7]. The initial model is fully convective and corresponds to

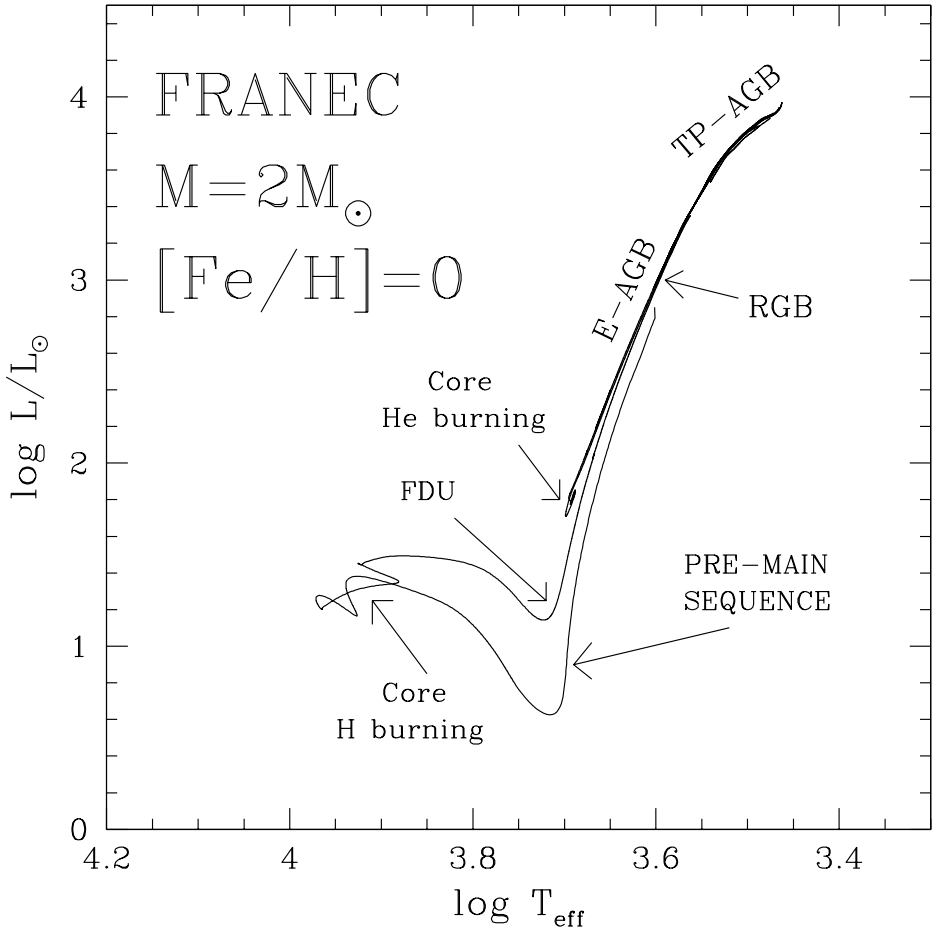

Fig. 2. Theoretical evolutionary track in the Hertzsprung-Russell diagram of a star of initial mass $M = 2\ M_{\odot}$ and solar metallicity (see section 9 for details of the model).

the pre-main sequence contraction phase, with a central temperature of about 10^5 K. The model has been evolved from the pre-main sequence, through core H burning, the red giant branch (RGB), the off-center He flash and the He burning, up to the AGB.

After the star leaves the main sequence and first becomes a red giant, the convective envelope penetrates in the radiative region above the H shell, enriching

[2] These values of Y and Z have been derived from a standard solar model, by fitting the luminosity ($L_{\odot} = 3.844 \cdot 10^{33}$ erg/s), radius ($R_{\odot} = 6.951 \cdot 10^{10}$ cm) and the mass fraction of metals relative to hydrogen ($(Z/X)_{\odot} = 0.017$) of the present Sun.

the surface composition with the ashes of proton captures that occurred in this deep zone during the main sequence (first dredge up, FDU); with respect to the pristine composition, ^{4}He, ^{3}He, ^{13}C, ^{17}O, and ^{14}N are enhanced, while ^{12}C, ^{15}N and ^{18}O are depleted (see e.g. [15]). Light elements, Li and Be, are practically extinguished. The upper mass limit for the occurrence of the first dredge up increases with the metallicity. At $Z = 0.02$, all stars entering the AGB have experienced the first dredge up episode, but this only occurs for $M < 3\ M_{\odot}$ and $M < 2.5\ M_{\odot}$ when $Z = 0.001$ and 0.0001, respectively ([15], [38]).

During the first part of the asymptotic giant branch (called early-AGB), the He shell burning progressively moves outward and the mass of the C-O core increases. In low mass stars, the H burning maintains an entropy barrier that limits the internal boundary of the external convective layer. In contrast, in massive AGB stars, owing to the huge energy flux coming out from the He burning zone, the base of the H-rich envelope expands and cools, so that the H burning dies down. In this case, the external convection penetrates inward, within the H-depleted zone. This is the second dredge up (SDU), found in stellar models with $M > 3{-}5\ M_{\odot}$, depending on the chemical composition [3]. As a consequence of the SDU, a further increase of the surface abundances of helium and nitrogen is expected in massive AGBs. In addition, the SDU reduces the H-depleted region and prevents the formation of massive white dwarfs.

Finally, when the He burning shell gets closer to the H/He discontinuity, it dies down and, after a rapid contraction, the H burning shell fully supplies the surface energy loss.

3 Thermally pulsing AGB

The temporary stop of the He burning shell marks the beginning of the thermally pulsing AGB phase (TP-AGB). The first thermal pulse occurs when the H burning shell accumulates enough He below it, so that the He-rich zone is compressed and heated, and He reignites. Although the degree of electron degeneracy of the He-rich material is weak, a thermonuclear runaway occurs, because the thermodynamical time scale needed to locally expand the gas is much longer than the nuclear burning time scale of the 3α reaction [109]. Owing to the fast release of nuclear energy, the local temperature increases and the He burning luminosity blows up, in extreme cases to $10^{9}\ L_{\odot}$. The thermonuclear runaway drives the formation of a convective zone that extends

[3] the lower the metallicity, the smaller the minimum mass for the occurrence of the second dredge up.

from the region of the partial He burning to the H/He discontinuity (see Figure 3). At the base of this convective shell an incomplete He burning takes

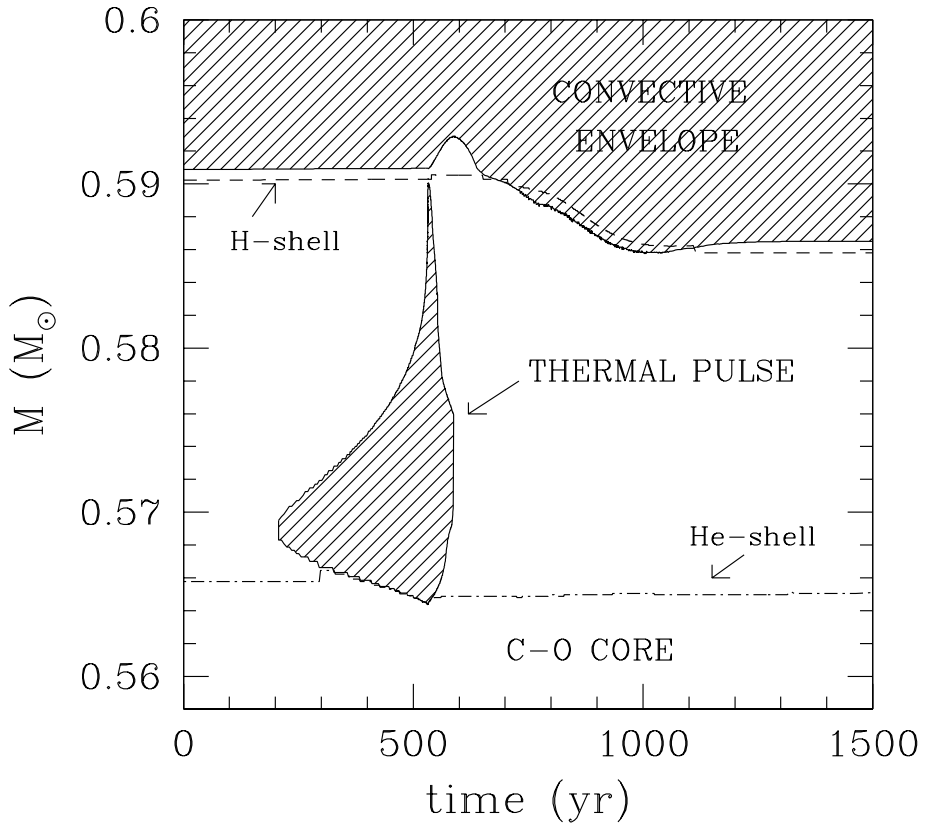

Fig. 3. Convective episode (dashed area) in the model of $M = 2\ M_\odot$, $Z = 0.015$ and $Y = 0.275$, during and after the $10^{\rm th}$ thermal pulse. Note how the convective zone generated by the thermal pulse covers the whole He intershell. After about 200 years, the external convection penetrates inward (TDU).

place and the products of the 3α reaction (essentially carbon) are mixed over the whole intershell. At the quenching of a thermal instability, the resulting mass fraction of C in the top layer of the He intershell is $X(^{12}{\rm C}) \sim 0.25$. When the expansion has progressed far enough, the temperature of the He shell decreases and a quiescent He burning phase begins. The variations of the H and He burning luminosities for the 2 $M_\odot$ model with $Z = 0.015$ are reported in Figure 4. The expansion powered by the thermal instability pushes outward the layers of material located above the He burning shell. The temperature and the density at the base of the H-rich envelope decrease and the H burning shell dies down. In these conditions, a third dredge up (TDU) episode is strongly favoured. Indeed, at the interface between the envelope and the mantel, owing to the large energy flux coming from below, the local temperature

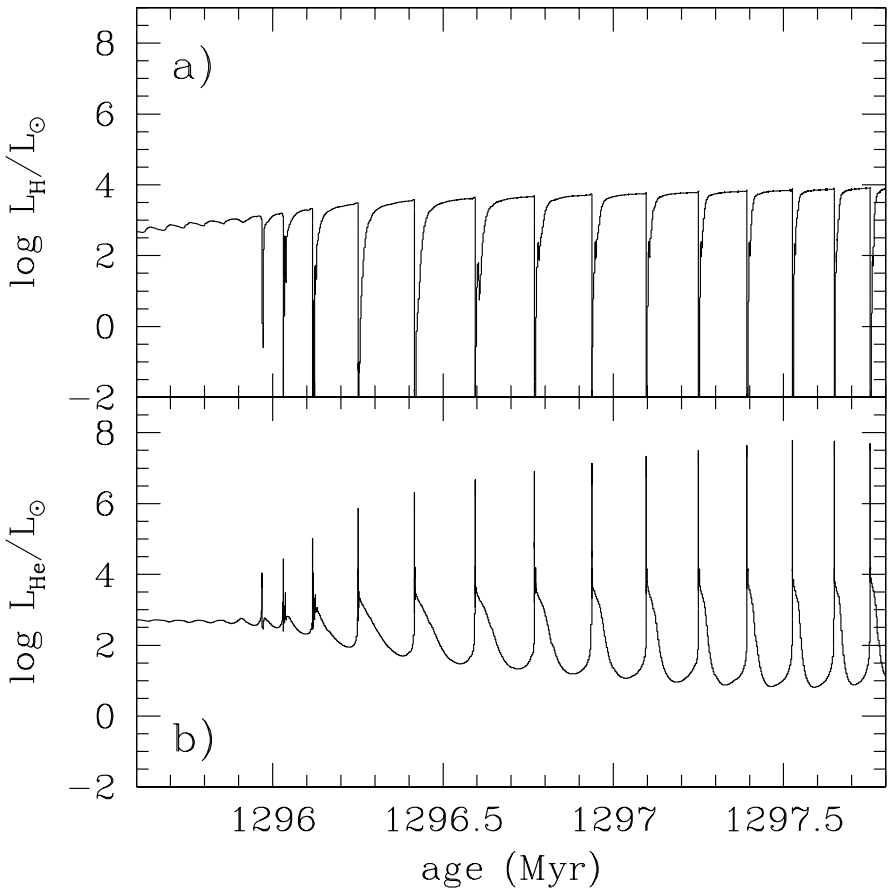

Fig. 4. Thermally pulsing AGB evolution of the model $M = 2\ M_\odot$, $Z = 0.015$ and $Y = 0.275$; panel a): energy production rate of the H burning shell; panel b): energy production rate of the He burning shell.

gradient increases. On the other hand, due to the low density, the ratio of the gas pressure to the radiation pressure decreases and the adiabatic temperature gradient approaches its minimum allowed value for a fully ionized gas plus radiation (i.e. $(d\log T/d\log P)_{ad} = 0.25$). Then the Schwarzschild criterion for the convective instability is more easily fulfilled and the envelope may penetrate (in mass) within the He intershell. The propagation of the convective instability is self-sustained due to the increase of the local opacity that occurs because fresh H (high opacity) is brought by convection into the He-rich layers (low opacity). If the dredge up is deep enough to overlap the region previously mixed by the convective zone generated by the TP, helium, carbon and heavy s elements are brought to the surface. A C(N) star may eventually form as a consequence of a series of recurrent TDU episodes ([67], [87], [113]).

Between two subsequent pulses (interpulse phase), the H burning shell supplies the energy radiated by the stellar surface and the luminosity of the star

basically depends on the mass of the H-exhausted core, $M_{\rm H}$. In other words, a direct correlation exists between the core mass and the stellar luminosity ([94], [69]) [4]. As the H burning shell advances in mass, the internal boundary of the convective envelope recedes, but always remains very close to the region where the thermonuclear reactions are switched on.

If the stellar mass is sufficiently large ($M \geq 5\ M_{\odot}$) [5], some nuclear processes are indeed active within the most internal layers of the convective envelope. In the more massive AGBs ($\sim 7\ M_{\odot}$), the temperature at the base of the convective envelope may reach 80×10^6 K. This phenomenon is called hot bottom burning (HBB) ([118], [64], [43]). The main consequences of the coupling of nuclear burning and external convection are: i) a substantial increase of the stellar luminosity, which deviates from the classical core mass-luminosity relation ([13], [14]); ii) a modification of the surface composition. In particular, most of the C dredged up is converted into N, a fact that prevents the formation of massive C(N)-stars. Moreover, the surface $^{12}C/^{13}C$ ratio approaches its equilibrium value (3.5) and an enhancement of Li is possible [104], [123], through the so-called Cameron-Fowler mechanism [23].

4 The third dredge up

The products of the s-process nucleosynthesis as well as those of the partial He burning can be actually observed only if the third dredge up takes place. The TDU is driven by the expansion of the envelope powered by a thermal pulse. It is deeper when the strength of the pulse, as measured by the maximum luminosity attained by the He burning, is stronger. In principle, the strength of the pulse depends on temperature and density of the He-rich layer at the epoch of the ignition. The higher is the density and the temperature at He ignition, the stronger the thermal pulse is. For this reason, since He is accumulated by the thermonuclear fusion occurring in the H burning shell at the base of the envelope, the H burning rate is among the most important quantities regulating the physical conditions of the point where He ignites. It follows that the third dredge up is influenced by the parameters affecting the H-burning rate such as, in particular, the metallicity, the mass of the H-exhausted core and the mass of the envelope ([136], [69], [115]). As a general rule, a slower H burning implies a higher density of the He-rich layer and, therefore, a stronger thermal pulse ensues. Such an occurrence suggests a few important considerations:

[4] The classical core mass-luminosity relation, as reported by [69], relates the maximum luminosity reached toward the end of the interpulse phase and the mass of the H-exhausted core, namely: $L_{max} = 5.925 \cdot 10^4 (M_H - 0.495)$.

[5] This lower limit is smaller at low metallicity.

i) along the AGB, the mass of H-depleted material that is dredged up in a single episode ($\delta M_{\rm TDU}$) initially increases, because the core mass increases, reaches a maximum and then decreases, when the mass loss erodes a substantial fraction of the envelope (see Figure 9);

ii) for given core and envelope masses, the TDU is deeper in low metallicity stars, because the H burning is less efficient. We found that $\delta M_{\rm TDU}$ ($Z = 0.002$) $\sim 2 \times \delta M_{\rm TDU}$ ($Z = 0.02$), for the same core and envelope mass. The relation of the TDU with the metallicity should be carefully considered when comparing disk AGB stars with metal-poor extragalactic AGB stars, like those belonging to the Magellanic Clouds or to the Dwarfs Spheroidals galaxies [37];

iii) there is a minimum envelope mass for which the TDU takes place. This minimum depends on the core mass and on the chemical composition of the envelope. We found that the TDU ceases when the envelope mass becomes smaller than $0.3 \div 0.5$ $M_{\odot}$ [115]. This implies that in stars of initial mass below a given threshold ($M < 1.2$ $M_{\odot}$), the residual envelope mass at the beginning of the thermally pulsing AGB is already too small and the TDU cannot takes place. As a matter of fact, AGB stars belonging to the Galactic Globular Clusters, whose initial mass are of the order of $0.8 - 0.9$ $M_{\odot}$, do not show the enhancement of C and s-elements, which is the signature of the TDU [112]. Similarly, at variance with their metal-rich disk counterparts, halo post-AGB stars do not show any significant enhancement of the s-elements [52].

5 Mass loss

During the AGB, the star may become unstable against large amplitude pulsations. Pulsations induce a compression of the gas and the resulting increase of the density of the cool atmospheric layers favours the formation of complex molecules and dust grains, which trap the outgoing radiation flux driving a strong wind. Mass loss could also be influenced by the environment, as in close binary systems or in crowded stellar populations, like the central region of Globular Clusters. Mass loss erodes the envelope causing important changes in the stellar properties. The duration of the AGB, the strength of the pulse, the efficiency of the third dredge up are a few examples of the quantities affected by the mass loss. The correct evaluation of the mass loss rate is also required to estimate the degree of chemical pollution of the interstellar medium ascribed to AGB stars.

The AGB mass loss rate may be estimated from infrared color indices or from molecular CO rotational lines measurements. The available data indicate that it ranges between 10^{-8} and 10^{-4} $M_{\odot}$/yr. In variable AGB stars, the larger

the period the larger the mass loss is. No other correlations between mass loss and stellar parameters (luminosity, mass, composition) have been clearly identified (see e.g. [133]). The poor knowledge of the actual mass loss rate is one of the major uncertainties of AGB stellar models. Much effort has been devoted to derive a suitable prescription for this phenomenon to be used in calculations of AGB evolutionary models. The Reimers' formula [6] was introduced to describe the mass loss in population II red giants [100] and the η parameter was calibrated according to the luminosity and color distribution of bright globular clusters stars ($\eta \sim 0.4$, [101]). Unfortunately an equally stringent constraint for the calibration of the mass loss rate in AGB stars is lacking. In principle, the mass loss rate may be adjusted in order to reproduce the observed luminosity functions of the AGB stellar population, or that of a sub-sample of AGBs, like the C(N)-stars. Another important constraint can be derived from the initial to final mass relation [132]. On the base of synthetic AGB models, [56] suggested that a Reimers' mass loss formula, with the parameter $\eta = 5$, provides a suitable reproduction of these observational constraints. Their method, however, only indicates the average mass loss rate, whereas the mass loss history remains largely unknown. Indeed [57] showed how different mass loss prescriptions may equally fulfil the same constraints. Our tests, which make use of detailed stellar models to reproduce similar observational constraints, show that the mass loss rate suggested by [56] may be adequate only for the more massive and/or more evolved AGB stars, but in low mass AGBs it is definitely too high.

A possible alternative method to estimate the mass loss rate is based on the observed correlation with the pulsational period (see e.g. [122]). Since the evolution of the pulsational period depends on the variations of radius, luminosity and mass, this relation provides a simple method to estimate the evolution of the total stellar mass from basic stellar parameters. In Figure 5 we have collected data for the mass loss rate versus period, as measured by various authors for O-rich (open circles) and C-rich (triangles and squares) AGB stars. Beside the evident spread of the data, three different regimes can be recognized: i) $P < 300$ days: moderate mass loss (roughly between 10^{-8} and 3×10^{-7} $M_{\odot}$/yr); ii) $300 < P < 1000$ days: exponential increase of the mass loss; iii) $P > 1000$ days: the mass loss approaches a maximum ($\sim 5 \times 10^{-5}$ $M_{\odot}$/yr), which roughly coincides with the expected radiation-pressure-driven limit [122]. The dot-dashed line in the figure represents the prescription by Vassiliadis & Wood [122]. It clearly underestimates the mass loss rate of short period variables, whilst for P ranging between 500 and 1000 days the mass loss appears too high by an order of magnitude. Thus, we have worked out a new relation (solid line), which provides a better calibration of the mass

[6] $\dot{M}(M_{\odot}/yr) = 1.34 \cdot 10^{-5} \cdot \eta \cdot \frac{L^{\frac{3}{2}}}{M \cdot T_{\rm eff}^2}$, where L and M are in solar units and the effective temperature in K.

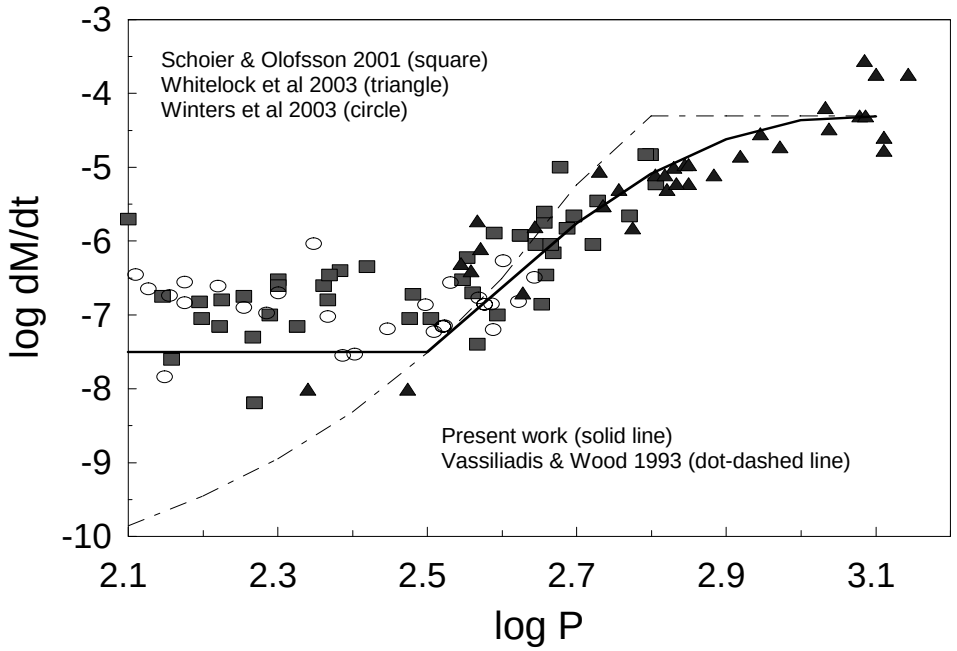

Fig. 5. Comparison of various mass loss rates versus period measurements (symbols) and prescriptions used in stellar evolution calculations (lines).

loss-period relation, namely:

for $\log P < 2.5$ $\quad \log\dot{M} = -7.7$

for $2.5 \leq \log P \leq 3.1$ $\quad \log\dot{M} = -101.6 + 63.26 \cdot \log P - 10.282 \cdot (\log P)^2$

for $\log P > 3.1$ $\quad \log\dot{M} = -4.3$

This prescription has been used in our latest calculations of low mass AGB stellar models. In Figure 6 we report the evolution of the envelope mass (M_{env}) of an AGB model of initial mass 2 $M_{\odot}$, as obtained under different prescriptions for the mass loss, namely: Reimers ($\eta = 5$), Reimers ($\eta = 0.5$), Vassiliadis & Wood (VW) and our new calibration of the mass loss-period relation (PW). The 0 of the temporal scale corresponds to the beginning of the TP-AGB phase. Note how the mass loss history depends on the rate prescription. While the Reimers' formula provides a constant increase of the mass loss, the Vassiliadis and Wood rate leads to a negligible mass loss for the major part of the AGB evolution, with a sudden increase to the radiation-pressure-driven limit toward the end. Our prescription resembles a moderate Reimers ($\eta = 0.5$) mass loss rate for the first 1.2 Myr and switches to the stronger $\eta = 5$ in the late TP-AGB phase. Note how the different prescriptions affect the duration of the AGB and, in turn, the AGB luminosity function and the estimated contribution of AGB stars to the Galactic chemical evolution.

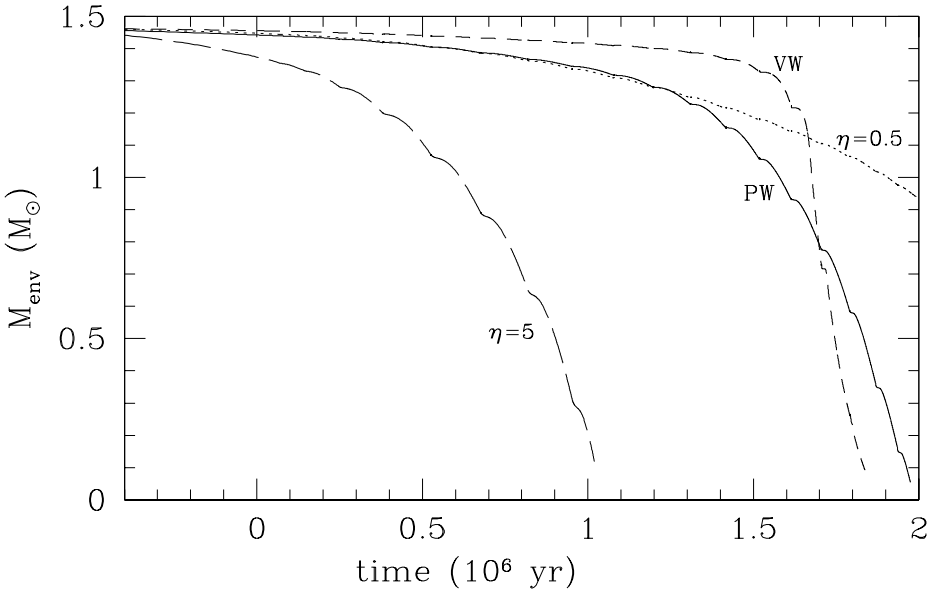

Fig. 6. Variation versus time of the envelope mass according to different mass loss prescriptions (see text), for an AGB model of initial mass $M = 2\ M_\odot$.

6 The source of neutrons and the formation of the ^{13}C pocket

As recalled in the Introduction, in thermally pulsing AGBs two major neutron sources may operate within the intershell, driven by the ^{22}Ne(α,n)^{25}Mg or by the ^{13}C(α,n)^{16}O reaction.

The amount of ^{14}N left by the H burning at the top of the intershell is practically equal to the sum of the abundances (by number) of the C-N-O in the envelope. During the early phase of the convective thermal pulse, the material within the intershell is fully mixed and the ^{14}N is totally converted into ^{22}Ne throughout the chain ^{14}N(α,γ)^{18}F($\beta^+\nu$)^{18}O(α,γ)^{22}Ne. Near the peak of the thermonuclear runaway, if the temperature is high enough (i.e. $\sim$3.5 $\times$ 10^8 K), the ^{22}Ne(α,n)^{25}Mg reaction may provide a significant neutron flux. Iben ([65]) first demonstrated that this condition is fulfilled in intermediate mass stars. Actually, in low mass stars ($M < 3\ M_\odot$), the temperature at the base of the convective zone generated by the TP barely attains 3 $\times$ 10^8 K and the ^{22}Ne neutron source is marginally activated ([70], [113], [49]).

In low mass AGB stars, an alternative neutron source is provided by the reaction ^{13}C(α,n)^{16}O. This reaction requires a substantially lower temperature, namely $\sim$90 $\times$ 10^6 K, which is easily attained in the He intershell. Note that between two subsequent thermal pulses, the H burning shell leaves some ^{13}C in the upper region of the He-rich intershell. The burning of this ^{13}C, however, produces a negligible neutron flux, even if, as a consequence of the TDU, the

CNO in the envelope may grow up to 10 times the solar abundance. This occurs because, in the material processed by the CNO burning, the ^{14}N is, in any case, two orders of magnitude more abundant than the ^{13}C. In practice, all the neutrons released by the ^{13}C left by the H burning are captured by the abundant ^{14}N. Then, an alternative source of ^{13}C is needed, in a zone where ^{14}N is depleted. The isotope ^{13}C is produced via ^{12}C(p,γ)^{13}N($\beta^+\nu$)^{13}C. After each thermal pulse, the material within the He-rich intershell is plenty of ^{12}C and all the ^{14}N has been converted into ^{22}Ne, but it is also H depleted. So, the problem is how to inject a few protons into the He-rich intershell.

Sackmann et al. [105] suggested that the convective zone generated by the thermal pulse could extend beyond the H/He discontinuity. In this case, protons are ingested downward, where the temperature is so high that the reaction chain ^{12}C(p,γ)^{13}N($\beta^+\nu$)^{13}C(α,n)^{16}O would release neutrons. Against this hypothesis, [66] argued that during the thermonuclear runaway the H burning shell remains active and generates an entropy barrier that prevents the penetration of the convective instability into the H-rich envelope. Extant AGB stellar models show that only in very metal-poor stars, owing to the lack of CNO, ingestion of protons in the convective pulse may occur ([47], [71], [114], [117]). More favorable conditions for the formation of a ^{13}C pocket within the intershell are realized at the epoch of the TDU and during the so-called post-flash dip, the period that immediately follows the TDU [69]. Indeed, as a consequence of the TDU, a sharp discontinuity between the H-rich envelope and the He- and C-rich intershell forms. This condition is maintained until H burning is reignited. The time elapsed from the maximum penetration of the convective envelope and H reignition is about 10^4 yr (for a star of 2 $M_\odot$). During this period, different physical mechanisms may contribute to the downward diffusion of a few protons into the underlying radiative layer. In such a case, at H reignition the top layers of the He intershell heat up and a ^{13}C pocket forms. Roughly speaking, the required mixing process must be able to diffuse about 10^{-6} $M_\odot$ of H within a region as large as $\sim 10^{-3}$ $M_\odot$. Note that an excess of protons must be avoided, because in that case the production of ^{13}C is followed by the production of ^{14}N (via the ^{13}C$(p,\gamma)^{14}$N reaction). Straniero et al. [116] demonstrated that the ^{13}C formed in this way is fully consumed by the ^{13}C(α,n)^{16}O reaction in radiative conditions during the interpulse phase, when the temperature rises up to $\sim 90 \times 10^6$ K, giving rise to a large neutron exposure with a maximum neutron density of about 10^7 cm^{-3}. The expected s-process nucleosynthesis has been first calculated by [49].

Among the various attempts to find the possible mechanism responsible for the formation of the ^{13}C pocket, [67] evaluated the timescale of the atomic diffusion driven by the sharp composition gradient left by the penetrating convective envelope at the time of the TDU and concluded that this is a promising possibility to diffuse enough protons from the envelope into the He-rich intershell. More recently [61], inspired by hydrodynamical simulations of

[45], invoked mechanical overshoot of material from the bottom of the convective envelope into the underlying stable region. Langer et al. [86] calculated AGB models taking into account stellar rotation and found a certain mixing of protons into the intershell at the epoch of the TDU. However, this rotationally induced mixing does not stop when the convective envelope recedes, but continues during the interpulse period causing the contamination of the ^{13}C pocket with too much ^{14}N. Gravity waves have been investigated to explain the formation of the ^{13}C pocket by [36], and [20] show that a magnetic field of 10^8 gauss, comparable with the one measured in white dwarfs, may induce a deep circulation below the convective envelope at the epoch of the TDU, allowing the required diffusion of protons into the intershell.

Owing to the lack of a reliable description of the physical phenomena that govern the diffusion of protons into the He intershell, in the current AGB nucleosynthesis calculations the amount of ^{13}C is assumed as free parameter (see [49]). In addition, the simultaneous solution of the stellar structure equations and a full network including all the relevant isotopes up to the termination point of the s-process path (Pb-Bi) requires a relevant computational power. For this reason, a post-process nucleosynthesis calculation, based on AGB stellar models computed with a restricted nuclear network, is generally preferred. In spite of these limitations, this approach provided a substantial improvement with respect to prior calculations, based on the so-called classical analysis of the s process (see discussion in [6]). The adequacy of detailed post-process calculations has been proved by comparing theoretical expectations with observed abundances found in galactic disk AGB stars ([84], [1], [2], [102], [17]). Additional confirmations have been derived from presolar SiC grains found in meteorites ([88], [106], [137]). These calculations are the bricks of the extant chemical evolution models incorporating heavy elements [120]. In general, observations show an important scatter of s-process abundances at any metallicity [19]. This scatter reveals a spread of the effective amount of ^{13}C in the pocket, perhaps due to differences in the stellar parameters, such as the initial mass or the mass loss rate, or to the chaotic nature of the process responsible of the proton injection into the He intershell.

7 The nuclear network

The next step in the understanding of the s-process nucleosynthesis in AGB stars is the development of algorithms that allow the formation of the ^{13}C pocket and a full coupling of the equations describing the physical and the chemical evolution of the star. In this framework, we have included a full network of about 500 isotopes (from H to the Pb-Bi-Po ending point) linked by more than 750 reactions, in the stellar evolution code FRANEC [28]. This network, the same already used in the post-process calculations, is continuously

upgraded according to the latest theoretical and experimental nuclear physics improvements. The adopted nuclear reactions are summarized in the following five subsections.

7.1 Charged particle capture reactions

Reaction rates of isotopes involving charged particles are generally taken from the NACRE compilation [5]. For those reactions not included in this database, we use the rates tabulated by [27]. Two important exceptions should be recalled. Concerning ^{14}N(p,γ)^{15}O, we use the result of the recent measurement obtained by the LUNA collaboration [44]. Being the bottleneck of the CNO cycle, this reaction regulates the He deposition on the intershell of an AGB star and in turn affects the pulse strength and the efficiency of the TDU (see the discussion in section 4). The new low energy astrophysical factor ($S(0)$=1.7 MeV barn) is about 40% lower than that suggested by NACRE. With regard to ^{12}C$(\alpha,\gamma)^{16}$O we adopt the rate recently derived by [83]).

7.2 Neutron sources

A subthreshold resonance makes difficult the low energy extrapolation of the ^{13}C(α,n)^{16}O reaction rate. We adopt the rate suggested by [41]. We have also investigated the effects of different rates ([82], [5]) and we found a negligible modification of the final surface isotopic distribution ([34], see also, [95]). The ^{22}Ne(α,n)^{25}Mg rate is even more complex, owing to the possible existence of unknown low energy resonances [77]. We adopted the lower limit suggested by [74]. It does not include the possible resonance at 633 keV and adopt a 1 σ lower limit (164 μeV) for the strength of the resonance at 828 keV. The recommended value by the NACRE compilation at $T \sim 3 \times 10^8$ K is a factor of two lower than our adopted choice, and very close to the recent determination of [72]. With such a rate, only a few neutron-rich isotopes involved in branchings sensitive to the peak neutron density, like ^{86}Kr, ^{87}Rb, ^{96}Zr, would be affected.

7.3 n-capture reactions

With n-capture reactions we mean (n,γ), (n,α) and (n,p) processes. For the (n,γ) reactions, we adopt, as reference compilation, the recommended rates by [8] (hereafter BK2000). In that paper, experimental and theoretical data are critically revised and the reaction rates are listed as a function of the thermal energy from 5 to 100 keV. We recall that the typical thermal energy

at which the s-process nucleosynthesis occurs in AGB stars are 8 keV for the ^{13}C(α,n)^{16}O reaction and 23 keV for the ^{22}Ne(α,n)^{25}Mg reaction. For the few reactions not included in BK2000, we use the theoretical calculations of [97].

Starting from this database, we have upgraded the network with the most recent experimental results. With regard to Si isotopes we refer to [58], Cl isotopes to [59], ^{60}Ni to [33], ^{62}Ni to [96], ^{88}Sr to [81], Kr isotopes to [51], Xe isotopes to [99], Cd isotopes to [135], ^{139}La to [92], Pm isotopes to [98], ^{151}Sm and Eu isotopes to [12] and finally Pt isotopes to [78]. The rates of (n, α) and (n, p) reactions involving heavy isotopes are taken from RT2000. We adopted the (n, α) and (n, p) rates on light isotopes from various authors. In particular: the ^{14}N(n,p)^{14}C is taken from [80], the ^{17}O(n,α)^{14}C from [127], the ^{26}Al(n,p)^{26}Mg from [79], the ^{26}Al(n,α)^{23}Na from [126] and the ^{33}S(n,α)^{30}Si from [107]. The ^{35}Cl(n,p)^{35}S rate has been derived from [42], the ^{36}Cl(n,p)^{36}S and the ^{36}Cl(n,α)^{33}P from [125], the ^{37}Ar(n,p)^{37}Cl and the ^{37}Ar(n,α)^{34}S from [54]. The ^{39}Ar(n,α)^{36}S is from [53], while ^{41}Ca(n,p)^{41}K and ^{41}Ca(n,α)^{38}Ar are from [124].

7.4 β decay reactions

Weak interaction rates (electron captures, β and positron decays) are interpolated as a function of the temperature (from 10^7 K to 10^{10} K) and electron density (from 1 to 30 cm^{-3}). At temperatures lower than 10^7 K we assume a constant value equal to the terrestrial one. For isotopes up to ^{37}Ar, data have been taken from [93], with the exception of ^{7}Be [27] and the isomeric state of ^{26}Al, for which we refer to [32]. Concerning the unstable isotopes between ^{39}Ar and ^{45}Ca we use prescriptions by [48], while between ^{45}Ca and ^{64}Cu (excluding ^{63}Ni) we follow [85]. For ^{63}Ni and heavier isotopes we use the rates tabulated in [119], with the exceptions of ^{79}Se and ^{176}Lu, for which we refer respectively to [75] and [76]. For the few rates not included in any compilation, we use the terrestrial value.

7.5 Isomeric states

The existence of isomeric states of unthermalized isotopes leads to ramifications of the s-process flux ([131], [130]). In particular, branching points originated by the isomeric state of ^{26}Al, ^{85}Kr, ^{176}Lu and ^{180}Ta require particular attention.

Concerning ^{26}Al, the proton capture on ^{25}Mg is split in two distinct reactions: the first produces the ground state ^{26}Al^g (with terrestrial half life $T_{1/2} = 7.16$

$\times 10^5$ yr) and the second creates the isomer $^{26}\mathrm{Al}^m$ that almost istantaneously decays into ^{26}Mg.

Concerning ^{85}Kr, the neutron capture of ^{84}Kr to $^{85}\mathrm{Kr}^m$ has a 50% probability with respect the total cross section (at 30 keV, [10]). $^{85}\mathrm{Kr}^m$ has a non-zero probability to decay by internal conversion to its ground state (of 20%), thus leading to the following isomeric ratio (IR):

$$IR = \frac{\sigma(^{84}\mathrm{Kr}(n,\gamma)^{85}\mathrm{Kr}^m)}{\sigma_{tot}(^{84}\mathrm{Kr}(n,\gamma)^{85}\mathrm{Kr})} = 0.42\ . \tag{1}$$

Note that the β^- half life of $^{85}\mathrm{Kr}^m$ is 4.48 h, while that of $^{85}\mathrm{Kr}^g$ is 10.76 yr.

Concerning ^{175}Lu, below 20 keV we adopt the terrestrial isomeric ratio, namely:

$$IR = \frac{\sigma(^{175}\mathrm{Lu}(n,\gamma)^{176}\mathrm{Lu}^m)}{\sigma_{tot}(^{175}\mathrm{Lu}(n,\gamma)^{176}\mathrm{Lu})} = 0.11, \tag{2}$$

while above this energy, the partial thermalization through a mediating state should also be considered (see [76]) and we assumed an effective IR=0.5.

Finally, for the complex treatment of the branching between isomeric and ground state of ^{180}Ta, we refer to [90].

8 Mixing during the third dredge up and formation of the ^{13}C pocket

In the model presented here we adopt a simple approach based on an argument early discussed by [9] (see also [26], [46]). When the TDU takes place, the opacity of the envelope (H-rich) is significantly larger than the opacity of the underlying H-exhausted region (He-rich). This fact causes an abrupt change of the temperature gradient at the inner border of the penetrating convective envelope. In this condition, the convective boundary becomes unstable, because any perturbation causing an excess of mixing immediately leads to an increase of the opacity and, in turn, to an increase of the temperature gradient. This occurrence favours a deeper penetration of the convective instability or, in other words, a deeper dredge up. A similar mechanism is responsible for the growth of the convective core during central He burning ([94], [24]). A different view of the same phenomenon concerns the evaluation of the average convective velocity. In the framework of the mixing length theory, this velocity is proportional to the difference between the radiative temperature gradient (i.e. the gradient necessary to carry out the total energy flux if convection

would be inhibited) and the adiabatic temperature gradient. For this reason, the average convective velocity usually drops to 0 at the stable boundary of a convective layer, where the temperature gradient coincides with the adiabatic one. However, when convection penetrates in a region of lower opacity (as happens during a third dredge up episode), the difference between the actual temperature gradient and the adiabatic gradient grows above 0 and a positive average convective velocity is found at the inner border of the convective envelope, which, for this reason, becomes unstable. In principle, as soon as He is mixed with the envelope, the opacity and, in turn, the difference between the radiative and the adiabatic temperature gradients are reduced. However, the mass of the convective envelope is usually much larger than the amount of the dredged up material and the relaxing effect of the additional mixing is, in practice, negligible ([46], [25]). Then, a simple thermodynamic criterion cannot be used to determine the real extension of the convective instability. For sure, the steep pressure gradient that develops immediately below the formal border of the convective envelope limits the penetration of the instability, so that the average convective velocity should rapidly drop to 0. In order to mimic this behaviour, we assume that in the region underlying the formal convective boundary, the average velocity follows an exponential decline, namely:

$$v = v_{bce} \exp\left(-\frac{d}{\beta H_P}\right), \tag{3}$$

where d is the distance from the formal convective boundary, v_{bce} is the velocity of the most internal convective mesh, H_P is the pressure scale height and β is a free parameter. Note that this formula is similar to the "overshoot" proposed by [61]. However, in our case, since v_{bce} is usually 0, it produces a negligible amount of extra mixing, except during a dredge up.

Then, the degree of mixing is calculated by means of the following relation:

$$X_j = X_j^o + \frac{1}{M_{conv}} \sum\nolimits_k (X_k^o - X_j^o) f_{j,k} \Delta M_k \tag{4}$$

where the summation is extended over the whole convective zone and the superscript ^{o} refers to unmixed abundances. ΔM_k is the mass of the meshpoint k and M_{conv} is the total mass of the convective zone. The damping factor f is:

$$f_{j,k} = \frac{\Delta t}{\tau_{j,k}} \tag{5}$$

if $\Delta t < \tau_{j,k}$, or

$$f_{j,k} = 1 \tag{6}$$

if $\Delta t \geq \tau_{j,k}$. Here Δt is the time step and $\tau_{j,k}$ is the mixing turnover time between the mesh-points j and k, namely:

$$\tau_{j,k} = \int_{r(j)}^{r(k)} \frac{dr}{v(r)} = \sum\nolimits_{i=j,k} \frac{\Delta r_i}{v_i} \tag{7}$$

The mixing velocity (v_i) is computed according to the mixing length theory, except in the region where the exponential decline is assumed. This algorithm allows us to account for the partial mixing that occurs when the time step is reduced to or below the mixing timescale. In practice, when the third dredge up takes place, complete mixing is obtained within the fully convective zone, while the region immediately below, where the convective turnover time scale is larger, is only partially mixed. Figure 7 shows the chemical profile, the radiative and adiabatic temperature gradients, the average velocity and the pressure, in the region around the convective boundary, in a model of 2 $M_\odot$, during the 5^{th} dredge up episode (see section 9). The three major effects of the introduction of this exponential decay of the convective velocity are: i) the convective boundary is more stable against perturbation; ii) a smooth profile of protons within the intershell is left by the TDU; iii) a more efficient TDU results. As a consequence of ii), a ^{13}C pocket almost ^{14}N-free forms in this zone. After a few tests, we found that in order to get a suitable amount of ^{13}C in the pocket, the β parameter should be of the order of 0.1.

9 A thermally pulsing AGB model

The network and the mixing algorithm described in the previous sections have been used to calculate the evolutionary sequence of a 2 $M_\odot$ star of solar metallicity shown in Figure 2. Before the first thermal pulse, a Reimers' formula for the mass loss ($\eta = 0.4$) has been assumed. At this epoch, the total and the core masses are 1.95 and 0.55 $M_\odot$, respectively. During the thermally pulsing AGB phase, we use the mass loss rate prescription discussed in section 2.3 (see the solid line in Figure 6). The calculation has been stopped when the envelope mass was reduced down to ~ 0.3 $M_\odot$, the corresponding total mass being 0.92 $M_\odot$. At this epoch, the TDU ceases (see Figure 8) and hence the envelope composition no longer changes. Figure 8 illustrates the evolution of the mass coordinates of the maximum energy production within the He intershell, the maximum energy production within the H burning shell and the inner border of the convective envelope. The first TDU episode occurs after six TPs, when the core mass is 0.56 $M_\odot$. The evolution of $\delta M_{\rm TDU}$ (the amount of mass dredged up) and $T^{\rm TP}_{max}$ (the maximum temperature at the base of the convective zone generated by the thermal pulse) are reported in Figure 9. The

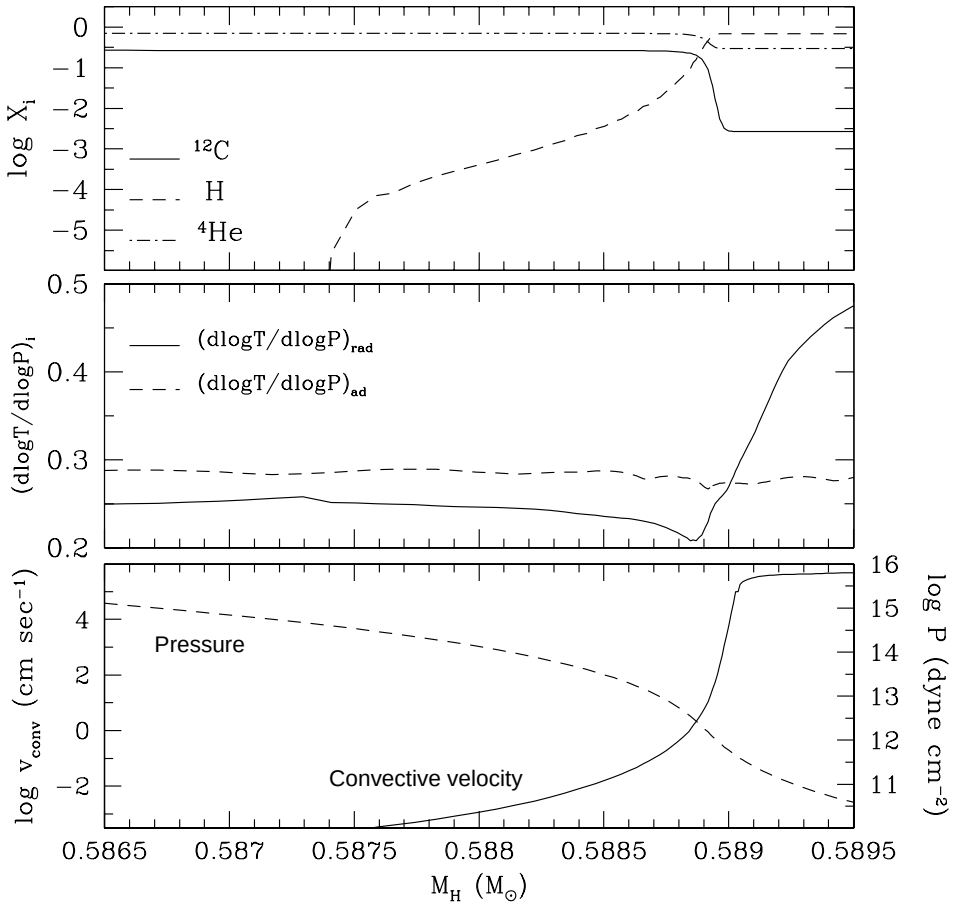

Fig. 7. Chemical profile (*upper panel*), temperature gradients (*middle panel*), average velocity and pressure (*lower panel*), in the region at the convective boundary during the fifth TDU episode.

possible activation of the ^{22}Ne(α,n)^{25}Mg reaction critically depends on $T^{\rm TP}_{max}$ that, for this reason, represents a key quantity for the comprehension of the nucleosynthesis occurring in AGB stars. It is obviously related to the maximum He burning luminosity. Then, as for the dredge up, the maximum temperature is a function of the core mass, the envelope mass and the composition [115]. As expected, the deepness of the third dredge up initially increases, due to the increase of the core mass. Then, during the TP-AGB phase, the effect of the envelope erosion becomes important, and the dredge up efficiency decreases, dropping to 0 after the last computed thermal pulse. C/O becomes larger than 1 when the core mass is about 0.6 $M_\odot$ and the luminosity is $\log L/L_\odot = 3.85$, which corresponds to a bolometric magnitude of -4.9 mag. We recall that the majority of the C(N) stars in the galactic disk have bolometric magnitudes around -5 mag. The final C/O is 1.67.

$T^{\rm TP}_{max}$ initially increases and attains a nearly asymptotic upper limit, of about

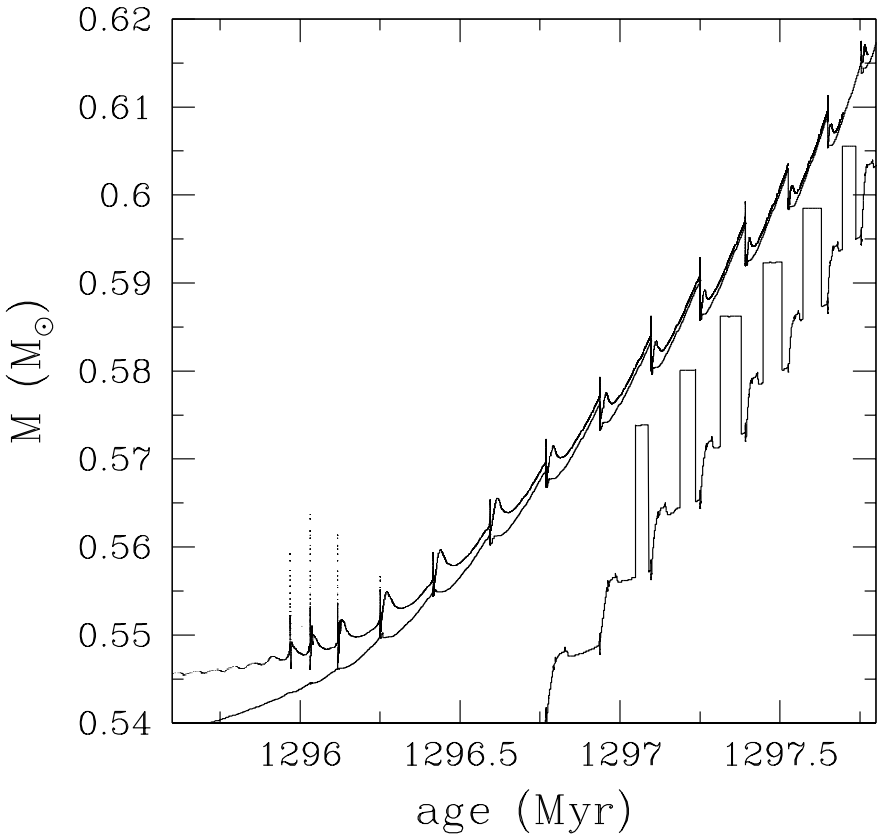

Fig. 8. The evolution throughout the TP-AGB phase of a star with initial mass M = 2 $M_\odot$ and solar metallicity. The three lines represent (from the top): the inner border of the convective envelope, the location of the maximum energy production within the H burning shell and the location of the maximum energy production within the He-rich intershell.

285 $\times$ 10^6 K. At such a low temperature the ^{22}Ne(α,n)^{25}Mg is marginally activated. On the contrary, an important s-process nucleosynthesis is driven by the ^{13}C(α,n)^{16}O reaction. A ^{13}C pocket forms after each TDU episode. The ^{13}C in the first two pockets is only partially burned during the interpulse and the residual is engulfed into the convective zone generated by the subsequent thermal pulse. In all other cases, the ^{13}C is fully consumed during the interpulse. The outward shift of the location of the maximum energy production within the intershell, in Figure 8, marks the onset of the ^{13}C burning during the interpulse. Figure 10 illustrates the various steps of the formation of the 4^{th} ^{13}C pocket. Note that the zone where the ^{13}C pocket forms (panel d)) is partially overlapped by a more external thin ^{14}N pocket. The maximum neutron density (about 10^7 cm^{-3}) is attained in the more internal layer of the ^{13}C pocket, where the ^{14}N is less abundant. The *effective* abundances of ^{13}C in all the pockets we found (defined as $X_{\rm eff}(^{13}{\rm C})$=$X(^{13}{\rm C})$ - $X(^{14}{\rm N})$ $\times$ 13/14) are reported in Figure 11. The extension of the pockets decreases with time, the first one beeing the largest.

The ashes of the neutron-capture nucleosynthesis allowed by the ^{13}C burning are spread within the intershell by the subsequent convective thermal pulse. Later on, as a consequence of the third dredge up, the envelope composition

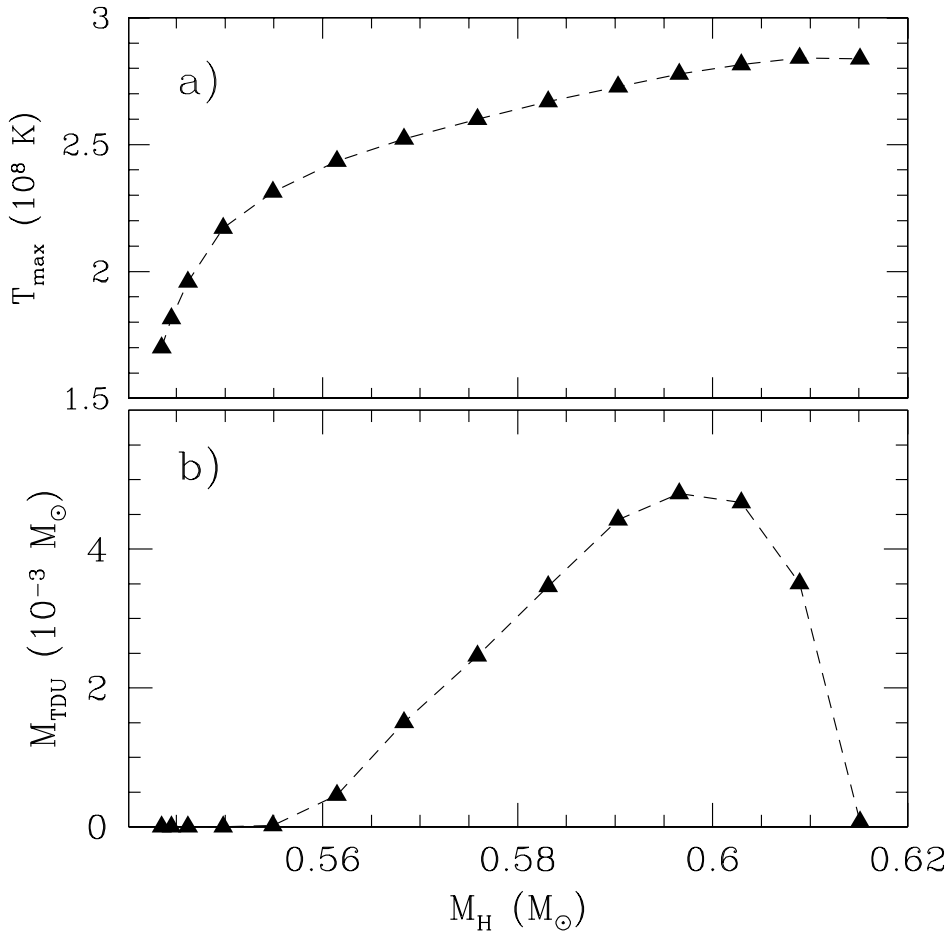

Fig. 9. Evolution of the maximum temperature at the base of the convective zone generated by the thermal pulse (panel a) and dredged up mass per pulse (panel b) during the AGB phase of the model of Figure 1.

is polluted with the products of the s process. The final surface composition resulting after nine TDU episodes is reported in Figure 12. Among the light elements, note the logarithmic enhancements of C (0.5 dex), F (0.3 dex), Ne (0.14 dex) and Na (0.12 dex). We recall that C is the main product of the 3α-burning. Fluorine is synthesized in the convective shell generated by the thermal pulse via the $^{15}N(\alpha,\gamma)^{19}F$ reaction, the ^{15}N being accumulated in the ^{13}C pocket mainly via the chain $^{14}N(n,p)^{14}C(\alpha,p)^{18}O(p,\alpha)^{15}N$ [7]. The nitrogen enhancement in the envelope (0.3 dex) is totally due to the first dredge up. In fact, the ^{14}N left by the H burning within the intershell is fully converted into ^{22}Ne during the convective thermal pulse, giving rise to the resulting Ne enhancement. The Na enhancement is partly due to the proton captures on ^{22}Ne, occurring within the H-burning shell, and partly due to the

[7] A minor contribution to the synthesis of the ^{15}N in the pocket may eventually come from the $^{14}N(n,\gamma)^{15}N$ and from the $^{14}N(p,\gamma)^{15}O$ reactions.

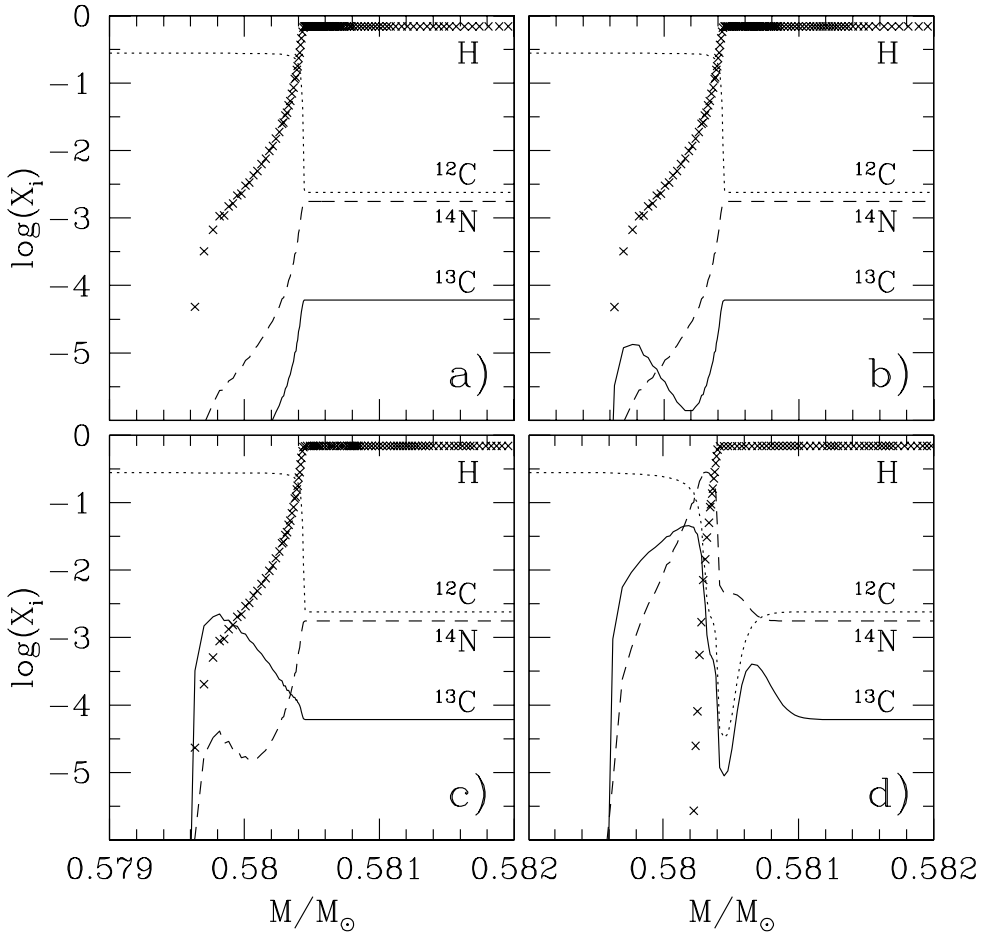

Fig. 10. The variation of the relevant chemical species in the region where the ^{13}C pocket forms after the occurrence of the third dredge up. Each panel refers to different time steps, namely: Δt = 78, 1000, 2000 and 14000 years, respectively.

neutron captures on ^{22}Ne followed by the ^{23}Ne decay, taking place within the He intershell. Concerning the s-process nucleosynthesis, all the elements (from Sr to Pb) are enhanced at various degree. We find that the abundance of Sr, Y and Zr at the first s peak, the so-called ls elements (*light* s elements), is comparable with the one of the hs elements (*heavy* s elements) Ba, La, Ce, Pr, Nd at the second s peak. Lead is underproduced with respect to barium, as expected for AGB stars of this metallicity (see next section). In Figure 13, the predicted [hs/ls] when (C/O=1) is compared to those measured in galactic C(N) giants [2]. Note that, for a given metallicity, this intrinsic index is indicative of the physical conditions of the s-process site.

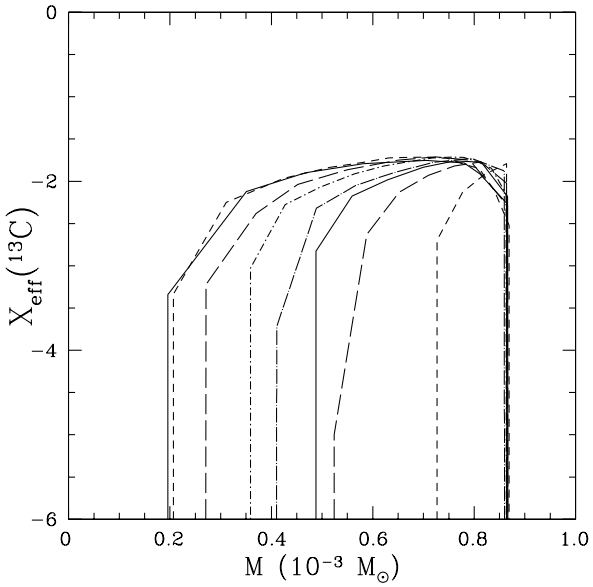

Fig. 11. The *effective* (see text) mass fraction of ^{13}C within all the pockets is reported. Each pocket has been shifted in mass in order to superimpose their external borders. The 0 point of the abscissa is arbitrary. The extension of the pocket decreases with time. The first is about $6.5 \cdot 10^{-4}$ $M_\odot$ large. The last is about 6 time smaller.

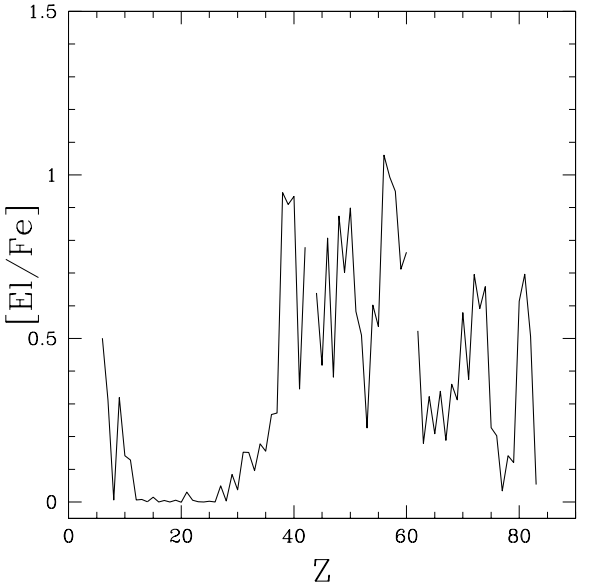

Fig. 12. Final surface composition of the model in Figure 1. The standard spectroscopic notation, namely [El/Fe]=log(N(El)/N(Fe))−log(N(El)/N(Fe))$_\odot$, is used, where El is the name of a generic element.

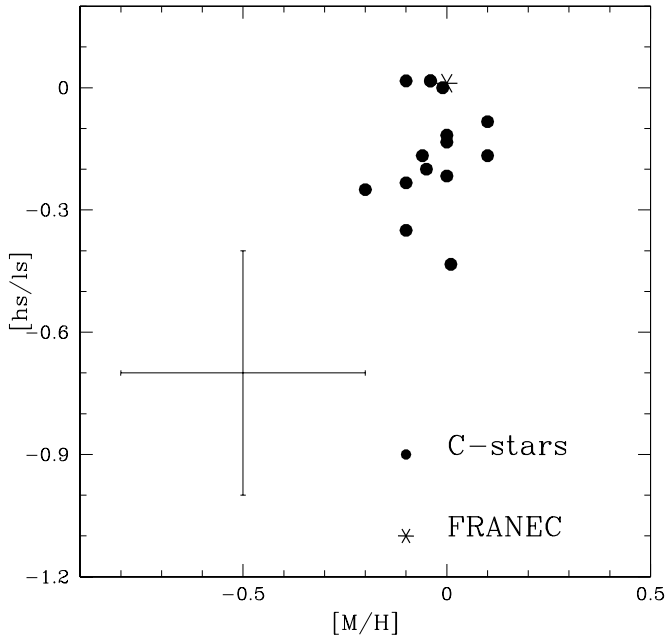

Fig. 13. Observed [hs/ls] ratio of a sample of galactic C(N) stars, compared with our theoretical prediction. The huge cross represents typical observational error bars of C(N) stars, whose spectra are very crowded (see [2]).

10 Nucleosynthesis in low-metallicity AGB stars: lead stars

The last challenging chapter of the AGB nucleosynthesis story is provided by the high resolution spectroscopy of very metal-poor C- and s-rich stars. The present generation of halo stars is old ($\sim$ 14 Gyr) and, therefore, is made of low mass objects ($M < 0.9\ M_{\odot}$). Then, when a low mass star reaches the AGB, its envelope is so small that the TDU never takes place. However, available spectroscopic surveys for very metal-poor stars ([11], [29]) found that $\sim$20% to 30% of the candidates ([Fe/H] > -2.5) are carbon rich. These stars are probably low mass dwarfs or giants, with a lifetime comparable with the age of the Galaxy, belonging to binary systems. It is possible that in most cases the C enhancement is the result of an ancient accretion process (by stellar wind or Roche lobe overflow [73]) from a more massive AGB companion (now a white dwarf). In such a case, also the products of the neutron capture nucleosynthesis were enhanced in the material accreted onto the secondary star.

In low mass AGBs, the main source of neutrons, the ^{13}C(α,n)^{16}O, is primary-like, i.e. not directly affected by the metallicity of the pristine material. Nevertheless, the iron seeds scale with the metallicity, so that the lower the metallicity the larger is the number of neutrons available per seed. As a result, at low metallicities, most of the seeds are converted into ^{208}Pb, at the termination point of the s-process fluence. Note that in stars suffering recurrent TDU

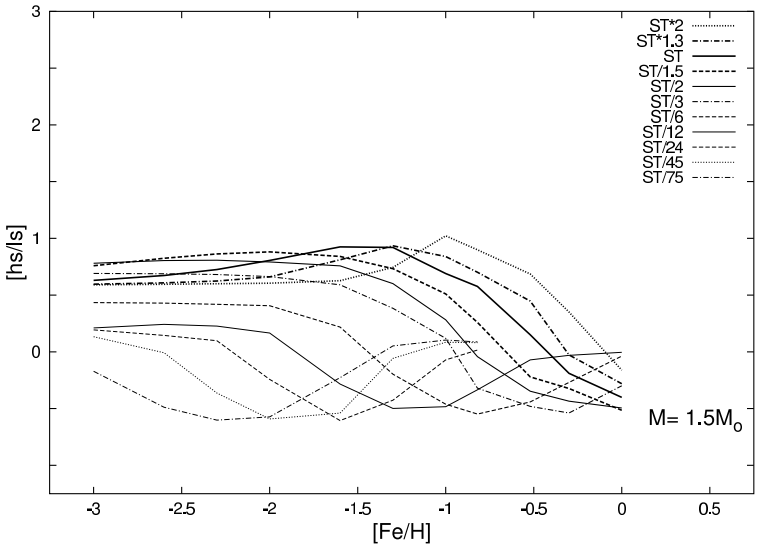

Fig. 14. Predicted [hs/ls] versus [Fe/H] for different ^{13}C pocket choices.

episodes, the amount of ^{12}C in the envelope increases with time. This primary carbon is mainly converted into ^{14}N, within the H-burning shell, and, later on, into ^{22}Ne, within the convective zone generated by a thermal pulse (see section 6). In very metal poor stars, the primary neon accumulated in the intershell becomes the main seed for the s process [30] (see also [55]). For these reasons, in a very metal-poor AGB star experiencing a few TDU episodes, a consistent enhancement of lead is expected [18]. High-resolution spectroscopy of very metal-poor C-rich stars largely confirms such a qualitative expectation. However, the precise prediction of the heavy element enhancements at the surface of the secondary star is more complex than previously sketched. We have to recall that we are looking at the intershell material that was mixed with the envelope of the primary AGB stars during the various TDU episodes and, later on, further diluted within the pristine material of the envelope of the secondary star. If this secondary star (actually the C-rich object presently detected), is evolved off the main sequence, this late dilution may be particularly efficient. In addition, the amount of mass accreted depends on the orbital parameters of the system that are, in most cases, unknown.

In this context, in order to investigate the efficiency of the s-process site, intrinsic indices [hs/ls] and [Pb/hs] are particularly useful ([50], [35]). The variation of these two indices with metallicity are shown in Figures 14 and 15. These calculations are based on a grid of older FRANEC models, where the Reimers's parameterisation ($\eta = 0.5$) was used and no velocity profile below the convective envelope was introduced. The n-capture nucleosynthesis was calculated with a post-process code that follows in detail the physical and thermodynamical structure of the He-rich intershell in the TP-AGB phase. After each third dredge up, diffusion of protons in a thin layer in the top re-

gion of the He-rich intershell was assumed. It gives rise to a ^{13}C pocket at H reignition; the amount of ^{13}C in the pocket and its profile in mass was taken as a free parameter. The standard case (ST, see [49]) was shown to reproduce the main s-process component in the solar system for low mass AGB stars and half-solar metallicity. The ^{13}C pocket efficiency was assumed identical for all thermal pulses followed by TDU. Neutrons released by the ^{13}C pocket are of primary origin, depending on proton captures on the freshly nucleosynthesised ^{12}C. Varying the metallicity, the s-process distribution changes because it depends on the number of neutron captured per seed and, at low metallicities, peaks at Pb, at the termination of the s-process path. As recalled in section 7.2, a large spread of ^{13}C pocket efficiencies is needed in order to explain the spectroscopic observations of MS-S-C(N) stars belonging to the galactic disk [19]. In Figures 14, 15, different lines correspond to different ^{13}C pockets, where the ST case was multiplied or divided by a given factor as indicated in the inset. The ST×2 case is an upper limit because ingestion of a larger abundance of protons would favour the ^{14}N production by proton capture on ^{13}C. As a comparison, spectroscopic measurements of C and s-rich metal-poor stars are reported in Figure 15. It results that for very metal-poor stars, [hs/ls] is weakly affected by a change of the efficiency of the ^{13}C pocket, while large spreads of [Pb/hs] are expected, in quite satisfactory agreement with observations. This is in accord with the large spread of ^{13}C pocket efficiencies required by the observation of MS-S-C(N) stars ([19], [1] and [2]).

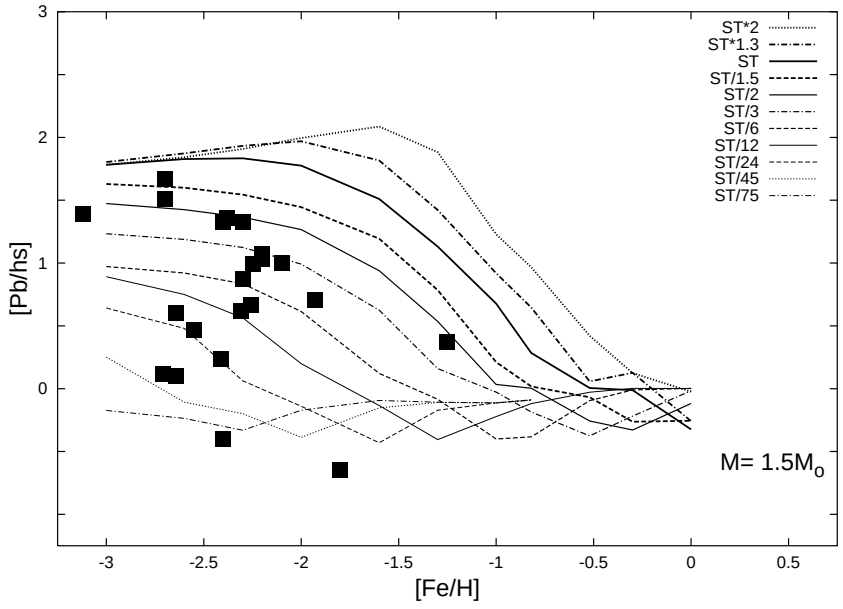

Fig. 15. Predicted [Pb/hs] versus [Fe/H] for different ^{13}C pocket choices. Spectroscopic data of s-rich and lead-rich stars are included for comparison (adapted from [35]).

Very low metallicity s-rich stars have an additional peculiarity: they are usually also N-rich. The enhancement of nitrogen could be due to the hot bottom

burning, but this would exclude low mass AGB stars that have a too cool temperature at the base of the convective envelope. The activation of the so-called cool bottom process during the AGB [91], a slow deep circulation taking place in the radiative region located between the H-burning shell and the inner border of the convective envelope, could contribute to the systematic occurrence of the nitrogen overabundance. More likely, [63] (see also [47]) suggested that the scarcity of CNO in very metal-poor stars may allow the convective zone generated by the first strong TP to ingest some protons from the envelope. In this case, a hot CN cycle would take place within the He-rich intershell and consistent amounts of ^{13}C and ^{14}N are produced. More recently [71], on the basis of detailed stellar models computations, proposed that a peculiar s-process nucleosynthesis, characterized by a high neutron density, could be activated by α-capture on the freshly synthesized ^{13}C. The detailed s-process nucleosynthesis for a low-mass and very metal-poor AGB model has been calculated by [114]. We found that the ingestion of proton into the convective intershell region and the subsequent deep TDU provide the required mechanism to explain the N enhancement, but the high neutron density is maintained only for a very short time (few days), with negligible consequences on the overall surface overabundances.

11 Conclusion.

We have reviewed the theoretical investigation of nucleosynthesis and evolution of low mass AGB stars. By introducing a full network (from H to Bi) in our stellar evolution code, we have obtained a self-consistent nucleosynthesis calculation for a 2 $M_{\odot}$ stellar model with solar composition.

Below the convective envelope of a thermally pulsing AGB star, the H burning, the He burning and the s process modify the internal composition. Then, the occurrence of recurrent third dredge up episodes induces the modification of the surface composition. The adoption of an exponential decay of the average convective velocity at the inner border of the convective envelope allows us to follow the formation of a ^{13}C pocket in the top layer of the He-rich intershell. During the interpulse, this pocket is compressed and heated, untill neutrons are released via the ^{13}C(α,n)^{16}O reactions. This is the main neutron source, responsible for the s-process nucleosynthesis in low mass AGB stars. A second (marginal) neutron burst, via the ^{22}Ne(α,n)^{25}Mg reactions, may eventually occurs at the base of the convective zone generated by a thermal pulse. One of the main source of uncertainty in modeling AGB stars concerns the choice of the mass loss rate. A new semiempirical calibration of the mass loss has been derived from a collection of the most recent observational data of variable AGB stars. This calibration has been used for the AGB model calculation presented here. We have followed the evolution up to the last third dredge up episode.

The final elemental distribution is representative of the one expected for the intrinsic carbon stars observed in the disk of the Milky Way. A comparison with available spectroscopic analysis shows a reasonable agreement.

40 years have passed since the discovery of the thermal pulses by Schwarzschild & Härm [109] and many efforts have been made for the comprehension of the AGB evolution and nucleosynthesis. The progressive improvement of the computational capability allows the development of more complex theoretical tools. The main tasks for the next future will be the comprehension of the role played by hydrodynamical phenomena usually neglected in standard stellar model computations (see e.g [39], [86], [91], [20], [62], [60]) and the refinement of the nuclear physics input data.

We wish to express our thanks to Debora Delaude and Marco Pignatari for helping in the preparation of this manuscript. We are indebted to Franz Käppeler and Inma Domínguez for a long profitable and continuous interaction. Part of this work has been supported by the Italian MIUR-FIRB Project "The Astrophysical Origin of the Heavy Elements beyond Iron" and by the Italian MIUR-PRIN Project 2004 "Nuclear astrophysics in low mass stars".

References

[1] Abia, C., Busso, M., Gallino, R., Domínguez, I., Straniero, O., Isern, J.: 2001, *ApJ* **559**, 1117.
[2] Abia, C., Domínguez, I., Gallino, R., Busso, M., Masera, S., Straniero, O., de Laverny, P., Plez, B., Isern, J.: 2002, *ApJ* **579**, 817.
[3] Allende Prieto C., Lambert D.L., Asplund M.: 2002, *ApJ* **573**, L137.
[4] Anders, E., Grevesse, N.: 1989, *Geochim. Cosmochim. Acta* **53**, 197.
[5] Angulo, C. and 27 coauthors: 1999, *Nucl. Phys. A* **656**, 3.
[6] Arlandini, C., Käppeler, F., Wisshak, K., Gallino, R., Lugaro, M., Busso, M., Straniero, O.: 1999, *ApJ* **525**, 886.
[7] Asplund, M., Grevesse, N., Sauval, A.J., Allende Prieto, C., Kiselman, D.: 2004, *A&A* **417**, 751.
[8] Bao, Z.Y., Käppeler, F.: 2000, *Atom. Data Nucl. Data Tables* **76**, 70.
[9] Becker, S.A., Iben, I.Jr.: 1979, *ApJ* **232**, 831.
[10] Beer, H.: 1991, *ApJ* **375**, 823.
[11] Beers, T.C.: 1999, in *ASP Conf. Ser.* **165**, 202.
[12] Best, J., Stoll, H., Arlandini, C., Jaag, S., Käppeler, F., Wisshak, K., Mengoni, A., Reffo, G., Rauscher, T.: 2001, *Phys. Rev. C* **64**, 0115801.
[13] Blöcker, T., Schönberner, D.: 1991, *A&A* **244**, L43.
[14] Boothroyd, A.J., Sackmann, I.-J: 1992, *ApJ* **393**, L21.
[15] Boothroyd, A.J., Sackmann, I.-J: 1999, *ApJ* **510**, 232.
[16] Burbidge, E.M., Burbidge, G.R., Fowler, W.A., Hoyle, F.: 1957, *Rev. of Mod. Phys.* **29**, 547.

[17] Busso, M., Gallino, R., Lugaro, M., Straniero, O., Smith, V.V., Lambert, D.L.: 2000, *Mem. Soc. Astron. It.* **71**, 805.
[18] Busso, M., Gallino, R., Wasserburg, G. J.: 1999, *ARA&A* **37**, 239.
[19] Busso, M., Gallino, R., Lambert, D.L., Travaglio, C., Smith, V.V.: 2001, *ApJ* **557**, 802.
[20] Busso, M., Nucci, M.C., Chieffi, A., Straniero, O.: 2004, *Mem. Soc. Astron. It.*, **75**, 648.
[21] Cameron, A.G.W.: 1954, *Phys. Rep.* **93**, 932.
[22] Cameron, A.G.W.: 1960, *AJ* **65**, 485.
[23] Cameron, A.G.W., Fowler, W.A.: 1971, *ApJ* **164**, 111.
[24] Castellani, V., Chieffi, A., Straniero, O.: 1992, *ApJ* **78**, S517.
[25] Castellani, V., Giannone, P., Renzini, A.: 1971, *Ap&SS* **10**, 340.
[26] Castellani, V., Marconi, M., Straniero, O.: 1996, *A&A* **340**, 160.
[27] Caughlan, G.R., Fowler, W.A.: 1988, *Atom. Data Nucl. Data Tables* **40**, 283.
[28] Chieffi, A., Domínguez, I., Limongi, M., Straniero, O.: 2001, *ApJ* **554**, 1159.
[29] Chieffi, A., Limongi, M., Straniero, O.: 1998, *ApJ* **502**, 737.
[30] Christlieb, N.: 2003, *Rev. Mod. Astron.* **16**, 191.
[31] Clayton, D.D.: 1968, in *Principles of Stellar Evolution and Nuclosynthesis*, Chicago: The Univ. of Chicago Press.
[32] Coc, A., Porquet, M.G., Nowacki, F.: 2000, *Phys. Rev. C* **61**, 015801.
[33] Corvi, F., Fioni, G., Gunsing, F., Mutti, P., Zanini, L.: 2002, *Nucl. Phys. A* **697**, 581.
[34] Cristallo, S., Straniero, O., Gallino, R.: 2004, in the Proceedings of the 8^{th} *Nuclei in the Cosmos Workshop*, *Nucl. Phys. A*, in press.
[35] Delaude, D., Gallino, R., Cristallo, S., Straniero, O., Husti, L., Ryan, S.: 2004, *Mem. Soc. Astron. It.*, **75**, 706.
[36] Denissenkov, P.A., Tout, C.A.: 2003, *MNRAS* **340**, 722.
[37] Domínguez, I., Abia, C., Straniero, O., Cristallo, S., Pavlenko, Ya-V.: 2004, *A&A* **422**, 1045.
[38] Domínguez, I. Chieffi, A., Limongi, M., Straniero, O.: 1999, *ApJ* **524**, 226.
[39] Domínguez, I., Straniero, O., Tornambé, A., Isern, J.: 1996, *ApJ* **472**, 783.
[40] Domínguez, I., Tornambé, A., Isern, J.: 1993, *ApJ* **419**, 268.
[41] Drotleff, H.W., Denker, A., Knee, H., Soine, M., Wolf, G., Hammer, J.W., Greife, U., Rolfs, C., Trautvetter, H.P.: 1993, *ApJ* **414**, 735.
[42] Druyts, S., Wagemans, C., Geltenbort, P.: 1994, *Nucl. Phys. A* **573**, 291.
[43] Forestini, M., Charbonnel, C.: 1997, *A&AS* **123**, 241.
[44] Formicola, A. and 31 coauthors: 2004, *Phys. Lett. B* **591**, 61.
[45] Freytag, B., Ludwig, H.-G, Steffen, M.: 1996, *A&A* **313**, 497.
[46] Frost, C.A., Lattanzio, J.C.: 1996, *ApJ* **473**, 383.
[47] Fujimoto, M.Y., Ikeda, Y., Iben, I.Jr.: 2000, *ApJ* **529**, L25.
[48] Fuller, G.M., Fowler, W.A., Newman, M.J.: 1982, *ApJS* **48**, 279.

[49] Gallino, R., Arlandini, C., Busso, M., Lugaro, M., Travaglio, C., Straniero, O., Chieffi, A., Limongi, M.: 1998, *ApJ* **497**, 388.
[50] Gallino, R., Delaude, D., Husti, L., Cristallo, S., Straniero, O., Ryan, S.: 2004, in the Proceedings of the 8^{th} *Nuclei in the Cosmos Workshop*, *Nucl. Phys. A*, in press.
[51] Gallino, R., Lugaro, M., Mutti, P., Straniero, O., Reifarth, R., Käppeler, F., Lewis, R.S., Davis, A.M., Wagemans, J.: 2002, in the Proceedings of the 11^{th} *Workshop on Nuclear Astrophysics*, eds. W. Hillebrandt & E. Müller, Garching: MPA/P13, 205.
[52] Giridhar, S., Lambert, D.L., Gonzalez, G.: 2000, *ApJ* **531**, 521.
[53] Goeminne, G.: 2001, PhD Thesis
[54] Goeminne, G., Wagemans, C., Wagemans, J., Geltenbort, P., Loiselet, M., Gaelens, M., Denecke, B., Koester, U.: 2001, *Nucl. Phys. A* **688**, 233.
[55] Goriely, S., Siess, L: 2001, *A&A* **378**, 25.
[56] Groenewegen, M.A.T., de Jong, T.: 1993, *A&A* **267**, 410.
[57] Groenewegen, M.A.T., de Jong, T.: 1994, *A&A* **282**, 127.
[58] Guber, K.H., Koehler, P.E., Derrien, H., Valentine, T.E., Leal, L.C., Sayer, R.O., Rauscher, T.: 2003, *Phys. Rev. C* **67**, 062802.
[59] Guber, K.H., Sayer, R.O., Valentine, T.E., Leal, L.C., Spencer, R.R., Harvey, J.A., Koehler, P.E., Rauscher, T.: 2002, *Phys. Rev. C* **65**, 058801.
[60] Herwig, F.: 2004, *ApJS* **155**, 651.
[61] Herwig, F., Blöcker, T., Schönberner, D., El Eid, M.: 1997, *A&A* **324**, L81.
[62] Herwig, F., Langer, N., Lugaro, M.: 2003, *ApJ* **593**, 1056.
[63] Hollowell, D., Iben, I.Jr., Fujimoto, M.Y.: 1990, *ApJ* **351**, 245.
[64] Iben, I.Jr.: 1973, *ApJ* **185**, 209.
[65] Iben, I.Jr.: 1975, *ApJ* **196**, 525.
[66] Iben, I.Jr.: 1976, *ApJ* **208**, 165.
[67] Iben, I.Jr.: 1982, *ApJ* **260**, 821.
[68] Iben, I.Jr.: 1983, *ApJ* **275**, 65.
[69] Iben, I.Jr., Renzini, A.: 1983, *ARAA* **21**, 271.
[70] Iben, I.Jr., Truran, J.W.: 1978, *ApJ* **220**, 980.
[71] Iwamoto, N., Kajino, T., Mathews, G.J., Fujimoto, M.Y., Aoki, W.: 2004, *ApJ* **602**, 377.
[72] Jaeger, M., Kunz, R., Mayer, A., Hammer, J.W., Staudt. G., Kratz, K.-L., Pfeiffer, B.: 2001, *Phys. Rev. Lett* **87**, 202501.
[73] Jorissen, A., Mayor, M.: 1992, *A&A* **360**, 115.
[74] Käppeler, F., Wiescher, M., Giesen, U., Goerres, J., Baraffe, I., El Eid, M., Raiteri, C.M., Busso, M., Gallino, R., Limongi, M., Chieffi, A.: 1994, *ApJ* **437**, 396.
[75] Klay, N., Käppeler, F.: 1988, *Phys. Rev. C* **38**, 295.
[76] Klay, N., Käppeler, F., Beer, H., Schatz, G.: 1991, *Phys. Rev. C* **44**, 2839.

[77] Koehler, P.E.: 2002, *Phys. Rev. C* **66**, 055805.
[78] Koehler, P.E., Harvey, J.A., Guber, K.H., Winters, R.R., Raman, S.: 2002, *J. Nucl. Sci. and Technology Suppl.* **2**, 546.
[79] Koehler, P.E., Kavanagh, R.W., Vogelaar, R.B., Gledenov, Yu.M., Popov, Yu.P.: 1997, *Phys. Rev. C* **56**, 1138.
[80] Koehler, P.E., O'Brien, H.A.: 1989, *Phys. Rev. C* **39**, 1655.
[81] Koehler, P.E., Winters, R.R., Guber, K.H., Rauscher, T., Harvey, J.A., Raman, S., Spencer, R.R., Blackmon, J.C., Larson, D.C., Bardayan, D.W., Lewis, T.A.: 2000, *Phys. Rev. C* **62**, 055803.
[82] Kubono, S. and 15 coauthors: 2003, *Phys. Rev. Lett.* **90**, 062501.
[83] Kunz, R., Fey, M., Jaeger, M., Mayer, A., Hammer, J.W., Staudt, G., Harissopulos, S., Paradellis, T.: 2002, *ApJ* **567**, 643.
[84] Lambert, D.L., Smith, V.V., Busso, M., Gallino, R., Straniero, O.: 1995, *ApJ* **450**, 302.
[85] Langanke, K., Martinez Pinedo, G.: 2000, *Nucl. Phys. A* **673**, 481.
[86] Langer, N., Heger, A., Wellstein, S., Herwig, F.: 1999, *A&A* **346**, L37.
[87] Lattanzio, J.: 1989, *ApJ* **344**, L25.
[88] Lugaro, M., Davis, A.M., Gallino, R., Pellin, M.J., Straniero, O., Käppeler, F.: 2003, *ApJ* **563**, 186.
[89] Merrill, P.W.: 1952, *ApJ* **116**, 21.
[90] Nemeth, Zs., Käppeler, F., Reffo, G.: 1992, *ApJ* **392**, 277.
[91] Nollett, K.M., Busso, M., Wasserburg, G.J.: 2003, *ApJ* **582**, 1036.
[92] O'Brien, S., Dababneh, S., Heil, M., Käppeler, F., Plag, R., Reifarth, R., Gallino, R., Pignatari, M.: 2003, *Phys. Rev. C* **68**, 035801.
[93] Oda, T., Hino, M., Muto, K., Takahara, M., Sato, K.: 1994, *Atom. Data Nucl. Data Tables* **56**, 231.
[94] Paczynski, B.: 1970, *Acta Astron.* **20**, 47.
[95] Pignatari, M., Gallino, R., Käppeler, F., Wiescher, M.: 2004, in the Proceedings of the 8^{th} *Nuclei in the Cosmos Workshop*, *Nucl. Phys. A*, in press.
[96] Rauscher, T., Guber, K.H.: 2002, *Phys. Rev. C* **66**, 028802.
[97] Rauscher, T., Thielemann, F.K.: 2000, *Atom. Data Nucl. Data Tables* **75**, 1.
[98] Reifarth, R., Arlandini, C., Heil, M., Käppeler, F., Sedyshev, P.V., Mengoni, A., Herman, M., Rauscher, T., Gallino, R., Travaglio, C.: 2003, *ApJ* **582**, 1251.
[99] Reifarth, R., Heil, M., Käppeler, F., Voss, F., Wisshak, K., Becvár, F., Krticka, M., Gallino, R., Nagai, Y.: 2002, *Phys. Rev. C* **66**, 064603.
[100] Reimers, D.: 1975, *Mem. Soc. R. Sci. Liege,* 6^{e} *Ser.* **8**, 369.
[101] Renzini, A.: 1981, in *Physical Processes in Red Giants*, eds. I. Iben Jr., A. Renzini, Dordrecht: Reidel, 431.
[102] Reyniers, M., Van Winckel, H., Gallino, R., Straniero, O.: 2004, *A&A* **417**, 269.
[103] Ritossa, C., Garcia-Berro, E., Iben, I. Jr.: 1996, *ApJ* **460**, 489.
[104] Sackmann, I.-J, Boothroyd, A.J.: 1992, *ApJ* **392**, L71.

[105] Sackmann,I.-J, Smith, R.L., Despain, K.H.: 1974, *ApJ* **187**, 555.
[106] Savina, M.R., Davis, A. M., Tripa, C.E., Pellin, M.J., Gallino, R., Lewis, R.S., Amari, S.: 2004, *Science* **303**, 649.
[107] Schatz, H., Jaag, S., Linker, G., Steininger, R., Käppeler, F., Koehler, P.E., Graff, S.M., Wiescher, M.: 1995, *Phys. Rev. C* **51**, 379.
[108] Schöier, F.L., Olofsson, H.: 2001, *A&AS* **368**, 969.
[109] Schwarzschild, M., Härm, R.: 1965, *ApJ* **142**, 855.
[110] Schwarzschild, M., Härm, R.: 1967, *ApJ* **150**, 961.
[111] Secchi, A.: 1868, *Astronomische Nachrichten* **1737**, 9.
[112] Sneden, C., Ivans, I.I., Kraft. R.P.: 2000, *Mem. Soc. Astron. It.* **71**, 657.
[113] Straniero, O., Chieffi, A., Limongi, M., Gallino, R., Busso, M., Arlandini, C.: 1997, *ApJ* **478**, 332.
[114] Straniero, O., Cristallo, S., Gallino, R., Domínguez, I.: 2004, *Mem. Soc. Astron. It.*, **75**, 665.
[115] Straniero, O., Domínguez, I., Cristallo, S., Gallino, R.: 2003, *PASA* **20**, 389.
[116] Straniero, O., Gallino, R., Busso, M., Chieffi, A., Limongi, M., Salaris, M.: 1995, *ApJ* **440**, L85.
[117] Suda, T., Aikawa, M., Machida, M.N., Fujimoto, M.Y., Iben, I.Jr.: 2004, *ApJS* **611**, 476.
[118] Sugimoto, D.: 1971, *Prog. Theor. Phys.* **45**, 761.
[119] Takahashi, K., Yokoi, K.: 1987, *Atom. Data Nucl. Data Tables* **36**, 375.
[120] Travaglio, C., Gallino, R., Arnone, E., Cowan, J., Jordan, F., Sneden, C.: 2004, *ApJ* **601**, 864.
[121] Ulrich, R.K.: 1973, in *Explosive Nucleosynthesis*, eds. Schramm D.N. & Arnett W.D., Austin: University Texas Press, 139.
[122] Vassiliadis, E., Wood, P.R.: 1993, *ApJ* **413**, 641.
[123] Ventura, P., D'Antona, F., Mazzitelli, I.: 2000, *A&A* **363**, 605.
[124] Wagemans, C., Bieber, R., Weigmann, H., Geltenbort, P.: 1998, *Phys. Rev. C* **57**, 1766.
[125] Wagemans, C., Goeminne, G., de Smet, L., Wagemans, J.: 2003, *Nucl. Phys. A* **719**, 127.
[126] Wagemans, J., Wagemans, C., Goeminne, G., Geltenbort, P., Moens, A.: 2001, *Nucl. Phys. A* **696**, 31.
[127] Wagemans, J., Wagemans, C., Goeminne, G., Serot, O., Loiselet, M., Gaelens, M.: 2002, *Phys. Rev. C* **65**, 034614.
[128] Wallerstein, G., Iben, I.Jr., Parker, P., Boesgaard, A.M., Hale, G.M., Champagne, A.E., Barnes, C.A., Käppeler, F., Smith, V.V., Hoffman, R.D., Timmes, F.X., Sneden, C., Boyd, R.N., Meyer, B.S., Lambert, D.L.: 1997, *Rev. Mod. Phys.* **69**, 995.
[129] Wallerstein, G., Knapp, G.R.: 1998, *ARA&A* **36**, 369.
[130] Ward, R.A., Newman, M.J.: 1978, *ApJ* **219**, 195.
[131] Ward, R.A., Newman, M.J., Clayton, D.D.: 1976, *ApJS* **31**, 33.
[132] Weidemann, V.: 2000, *A&A* **363**, 647.
[133] Whitelock, P.A., Feast, M.W., van Loon, J.Th., Zijlstra, A.A.: 2003,

MNRAS **342**, 86.
[134] Winters, J.M., Le Bertre, T., Jeong, K.S., Nyman, L.-A., Epchtein, N.: 2003, *A&A* **409**, 715.
[135] Wisshak, K., Voss, F., Käppeler, F., Kazakov, L.: 2002, *Phys. Rev. C* **66**, 025801.
[136] Wood, P.R.: 1981, in *Physical Processes in Red Giants*, eds. I. Iben Jr., A. Renzini, Dordrecht: Reidel, 135.
[137] Zinner, E.: 1999, *Ann. Rev. Earth Planet. Sci.* **26**, 147.